

Using SPTpol, Planck 2015, and non-CMB data to constrain tilted spatially-flat and untilted non-flat Λ CDM, XCDM, and ϕ CDM dark energy inflation cosmologies

Chan-Gyung Park¹ and Bharat Ratra²

¹*Division of Science Education and Institute of Fusion Science,
Jeonbuk National University, Jeonju 54896, Republic of Korea*

²*Department of Physics, Kansas State University,
116 Cardwell Hall, Manhattan, KS 66506, USA**

(Dated: March 27, 2020)

We use six tilted spatially-flat and untilted non-flat dark energy cosmological models in analyses of South Pole Telescope polarization (SPTpol) cosmic microwave background (CMB) data, alone and in combination with Planck 2015 CMB data and non-CMB data, namely, the Pantheon Type Ia supernovae apparent magnitudes, a collection of baryon acoustic oscillation data points, Hubble parameter measurements, and growth rates. Although the cosmological models that best-fit the Planck CMB and non-CMB data do not provide good fits to the SPTpol data, with the χ^2 's exceeding the expected value, given the uncertainties, in each model the cosmological parameter constraints from the SPTpol data and from the Planck CMB and non-CMB data are largely mutually consistent. When the smaller angular scale SPTpol data are used jointly with either the Planck data alone or with the Planck CMB and the non-CMB data to constrain untilted non-flat models, spatially-closed models remain favored over their corresponding flat limits. When used in conjunction with Planck data, non-CMB data (baryon acoustic oscillation measurements in particular, from six experiments) have significantly more constraining power than the SPTpol data.

PACS numbers: 98.80.-k, 95.36.+x

I. INTRODUCTION

A main goal of cosmology research is to use astronomical observations to measure the parameters of the cosmological model as accurately as possible. The currently widely accepted standard model is the spatially-flat Λ CDM model, [1], where the cosmological constant (Λ) dark energy and the cold dark matter (CDM) constitute 95% of the present energy content of the Universe with baryonic matter contributing the remaining 5% and the structure of the Universe has grown under gravitational instability from primordial infinitesimal quantum-mechanical energy density perturbations generated during the very early epoch of near slow-roll inflation. The main observations that lend significant support to this standard model include CMB anisotropy data [2, 3], Type Ia supernovae redshift-magnitude data [4], baryonic acoustic oscillations (BAO) data [5–10], and Hubble parameter [$H(z)$] measurements [11, 12].

Although the spatially-flat model with a time-independent cosmological constant as dark energy is widely accepted, the possibility still remains that space is not flat and that the dark energy is dynamical. Recent joint analyses of the Planck 2015 CMB and non-CMB observations in the untilted non-flat Λ CDM model show evidence for spatial non-flatness with 5.2σ significance [13–15]. Here the untilted non-flat model does not have the density perturbation power spectral index n_s as a free parameter, unlike in the commonly used

tilted spatially-flat model. Also, the Planck CMB and non-CMB observational data do not rule out the possibility of dark energy being dynamical, [13, 16–18]. Recent research also demonstrates that non-flat dynamical dark energy models with constant dark energy equation of state (XCDM) or based on a minimally coupled scalar field (ϕ CDM) [19] are still allowed by the current observations [13, 17, 20–22]. In the XCDM parameterization the dark energy density decreases with time. Here the dark energy is modeled as an ideal X -fluid with equation of state $p_X = w\rho_X$ where p_X and ρ_X are the fluid pressure and energy density and the equation of state parameter $w < -1/3$. Since this is a widely-used parameterization, we also consider it here. However, it is incomplete and needs to be extended since it is unable to consistently describe the evolution of spatial inhomogeneities. On the other hand, the ϕ CDM model — in which a scalar field is used to model dynamical dark energy — is physically complete and consistent.

While Planck CMB data have been widely used to constrain cosmological models, there also exist several CMB data sets from higher-resolution ground-based CMB observatories such as the Atacama Cosmology Telescope (ACT; [23]) and the South Pole Telescope (SPT; [24]). For example, the South Pole Telescope provides information on the CMB temperature and polarization spatial anisotropies at angular scales much smaller than the range probed by the Planck satellite (SPTpol; [25]). It is essential to investigate whether the Planck CMB data and other high resolution observations are mutually consistent. There have been two comparisons of the cosmological constraints from the Planck data and the SPTpol data, both of which made use of the tilted flat Λ CDM

*Electronic address: park.chan.gyung@gmail.com, ratra@phys.ksu.edu

model. The SPTpol collaboration, [25], concluded that the Planck 2015 and SPTpol results are mildly inconsistent in this model, while the Planck collaboration, [3], concluded that the Planck 2018 and SPTpol results are not inconsistent. However, no such consistency check has been made for other simple cosmological models, such as the flat dynamical dark energy (Λ CDM and ϕ CDM) models and the non-flat Λ CDM, XCDM, and ϕ CDM models, so it is not known if the above results are model independent.

Here we constrain cosmological parameters in the tilted flat and untilted non-flat Λ CDM, XCDM, and ϕ CDM dark energy models using the recent SPTpol CMB data sets, and study the consistency between the best-fit models favored by the SPTpol data and those favored by the Planck 2015 CMB and the non-CMB data [13, 17]. The non-CMB data used in our analysis includes the Pantheon Type Ia supernovae apparent magnitudes [4], a collection of BAO data points [5–10], Hubble parameter measurements, and growth rates [15]. Using a variety of cosmological models to compare different data sets has proved instructive, allowing somewhat model-independent conclusions to be drawn, [26]. We find that the constraints on model parameters from the SPTpol data and from the Planck CMB and the non-CMB data are not inconsistent and so we also derive constraints on cosmological parameters from joint analyses of all data.

The main “model-independent” conclusions of our analyses are: (i) All Planck CMB and non-CMB data best-fit cosmological models we study do not provide good fits to the SPTpol data. (ii) However, there is mutual consistency between the parameter constraints for a model that best fits the full SPTpol data and those for the same model that best fits the Planck CMB and the non-CMB data. (iii) When the full SPTpol data are used in joint analyses with either the Planck data alone or with the Planck CMB and the non-CMB data to constrain untilted non-flat models, closed models continue to be favored over their spatially-flat limits. (iv) When used together with Planck data, non-CMB data (BAO data in particular, from six experiments) have significantly more constraining power than do the SPTpol data.

This paper is organized as follows. Section II describes the observational data used in our analyses while Sec. III describes our method for constraining cosmological parameters of the six tilted flat and untilted non-flat Λ CDM, XCDM, and ϕ CDM models using various combinations of data sets. The inflation model power spectra, that define the cosmological models we use, are discussed in Sec. IV. Results are presented in Sec. V and a summary is provided in Sec. VI.

II. DATA

In this work, recent CMB and non-CMB data are used to constrain the tilted flat and untilted non-flat Λ CDM, XCDM, and ϕ CDM dark energy models. We use exactly

the same Planck CMB and non-CMB data sets used in Refs. [13, 17] for consistency with the previous works and to see what happens when the SPTpol data set is added to the mix.

We use the SPTpol and Planck 2015 CMB anisotropy data sets. The SPTpol data is composed of the CMB E -mode polarization angular power spectrum (EE) and the temperature- E -mode cross-power spectrum (TE) over the spherical harmonic multipoles $50 < \ell \leq 8000$, based on CMB temperature and polarization observations on 500 deg^2 of the sky [25]. Here we use three different SPTpol data sets, namely, TE+EE, TE, and EE band power measurements, and the corresponding covariance matrices, which are all publicly available at the South Pole Telescope website.

We also use the Planck 2015 CMB anisotropy data (TT+lowP) including the lensing data [2], where TT denotes the CMB temperature angular power spectrum at low ℓ ($2 \leq \ell \leq 29$) and high ℓ ($30 \leq \ell \leq 2508$) and lowP represents the low- ℓ CMB TE, EE, and BB polarization power spectra at $2 \leq \ell \leq 29$. The primary reason for using Planck TT+lowP CMB data is that TT+lowP data was the baseline power spectrum data for Planck 2015 analysis and that the same data was used in the SPTpol group analysis. One may think that the Planck CMB data with polarization at high ℓ should be used for fair comparison with the SPTpol data that span a wide range of ℓ . The parameters of the flat Λ CDM model constrained by Planck TT+lowP and TT,TE,EE+lowP data sets (with high- ℓ polarization information) are totally consistent with each other with deviation less than 0.2σ (see Table 3 of Ref. [2]). For the nonflat Λ CDM model, the deviation is less than 0.6σ [36]. Thus, it is valid to use the TT+lowP baseline power spectrum data when comparing with SPTpol data.

To get tighter constraints on model parameters, we jointly use the Planck and SPTpol data, together with non-CMB data. The non-CMB data sets we use are the Pantheon supernova Type Ia measurements (SN) [4], a compilation of BAO data [5–10], $H(z)$ measurements, and growth rates ($f\sigma_8$) (see Refs. [13, 17] for detailed description of these data).

In Table I, we summarize the BAO data points used in our analysis. Our collection encloses the BAO data sets adopted by the recent Planck 2018 data analysis [3]. Here $D_M(z)$ and $H(z)$ are the comoving distance and Hubble parameter at redshift z , respectively, $D_V(z) = [czD_M^2(z)/H(z)]^{1/3}$, $D_H(z) = c/H(z)$ with c the speed of light, r_d the sound horizon size at the drag epoch (z_d), and $f\sigma_8$ the growth rate. Note that the BAO data set of Ref. [5] includes Hubble parameters and growth rates as well as distance information and that in the actual analysis for the data points of Ref. [7, 10] the probability distributions instead of the approximate Gaussian constraints are used (see Sec. 2.3 of Ref. [15] for a more detailed description).

TABLE I: BAO measurements.

z_{eff}	Measurement	Reference
0.38	$D_M(r_d, \text{fid}/r_d)$ [Mpc] = 1512.39 ± 24.99	[5]
0.38	$H(r_d/r_d, \text{fid})$ [$\text{km s}^{-1} \text{ Mpc}^{-1}$] = 81.21 ± 2.37	[5]
0.51	$D_M(r_d, \text{fid}/r_d)$ [Mpc] = 1975.22 ± 30.10	[5]
0.51	$H(r_d/r_d, \text{fid})$ [$\text{km s}^{-1} \text{ Mpc}^{-1}$] = 90.90 ± 2.33	[5]
0.61	$D_M(r_d, \text{fid}/r_d)$ [Mpc] = 2306.68 ± 37.08	[5]
0.61	$H(r_d/r_d, \text{fid})$ [$\text{km s}^{-1} \text{ Mpc}^{-1}$] = 98.96 ± 2.50	[5]
0.38	$f\sigma_8 = 0.497 \pm 0.045$	[5]
0.51	$f\sigma_8 = 0.458 \pm 0.038$	[5]
0.61	$f\sigma_8 = 0.436 \pm 0.034$	[5]
0.106	$r_d/D_V = 0.327 \pm 0.015$	[6]
0.15	$D_V(r_d, \text{fid}/r_d)$ [Mpc] = 664 ± 25	[7]
1.52	$D_V(r_d, \text{fid}/r_d)$ [Mpc] = 3843 ± 147	[8]
2.33	$D_H^{0.7} D_M^{0.3}/r_d = 13.94 \pm 0.35$	[9]
2.36	$D_H/r_d = 9.0 \pm 0.3$	[10]
2.36	$D_A/r_d = 10.8 \pm 0.4$	[10]

Note: The sound horizon size (at the drag epoch) of the fiducial model is $r_{d, \text{fid}} = 147.78$ Mpc in [5] and [8], and $r_{d, \text{fid}} = 148.69$ Mpc in [7].

III. METHODS

We apply the Markov chain Monte Carlo (MCMC) method, implemented in a modified version of the CAMB/COSMOMC program (version of Nov. 2016) [27], to explore the parameter space of the dark energy inflation models. The CAMB program computes the matter and CMB power spectra based on the evolution of density perturbations of matter and radiation components and the COSMOMC program estimates the parameter constraints that are favored by the given observational data sets using the MCMC method.

The tilted flat Λ CDM model is characterized by six cosmological parameters ($\Omega_b h^2$, $\Omega_c h^2$, θ_{MC} , τ , A_s , n_s), where Ω_b and Ω_c are the current values of baryonic and cold dark matter density parameters, h is the Hubble constant H_0 in units of $100 \text{ km s}^{-1} \text{ Mpc}^{-1}$, θ_{MC} is the apparent size of the sound horizon at recombination defined in the CAMB/COSMOMC program, τ is the reionization optical depth, and A_s and n_s are the amplitude and the spectral index of the primordial scalar-type energy density perturbation power spectrum. In the tilted flat XCDM parameterization, we add one more free parameter, the equation of state parameter ($w = p_X/\rho_X$, where p_X and ρ_X are the pressure and energy density of the dark energy X -fluid). The X -fluid dark energy goes to the cosmological constant dark energy in the limit of $w = -1$. In the tilted flat ϕ CDM model where the scalar field potential energy density is given by $V(\phi) = V_0\phi^{-\alpha}$ [19], we instead add the positive slope parameter α as a

free parameter. The scalar field dark energy goes to the cosmological constant dark energy in the limit of $\alpha = 0$. In the untilted non-flat Λ CDM, XCDM, and ϕ CDM models, the spectral index n_s is replaced with the present value of the spatial curvature parameter Ω_k .

The background evolution of the Λ CDM, XCDM, and ϕ CDM dark energy models can be described by the evolution of the Hubble parameter. In the matter and dark energy dominated era, where the effect of radiation components can be ignored, the Hubble parameter at redshift z is given by

$$H^2(a) = H_0^2 (\Omega_m a^{-3} + \Omega_k a^{-2} + \Omega_\Lambda), \quad (1)$$

and

$$H^2(a) = H_0^2 (\Omega_m a^{-3} + \Omega_k a^{-2} + \Omega_X a^{-3(1+w)}), \quad (2)$$

for the Λ CDM and XCDM models, respectively. Here $a = 1/(1+z)$ is the cosmic scale factor normalized to unity at present, and $\Omega_m = \Omega_b + \Omega_c$ and Ω_Λ (Ω_X) are the present values of the matter and dark energy density parameters of the Λ CDM (XCDM) model, respectively. For the ϕ CDM model, the Hubble parameter can be written as

$$H^2(a) = \frac{H_0^2}{1 - \frac{1}{6}(\phi')^2} \left[\Omega_m a^{-3} + \Omega_k a^{-2} + \frac{V(\phi)}{3H_0^2} \right] \quad (3)$$

with the equation of motion of the dark energy scalar field

$$\phi'' + \left(3 + \frac{\dot{H}}{H^2} \right) \phi' + \frac{V_{,\phi}}{H^2} = 0, \quad (4)$$

where $\phi' \equiv d\phi/d\ln a$ and $V_{,\phi} = -V_0\alpha\phi^{-\alpha-1}$. Unlike in the Λ CDM and XCDM models, in the ϕ CDM model we use the Hubble constant (H_0) as a free parameter instead of θ_{MC} because the latter parameter is not suitable for use in some extreme situations where for larger values of α the scalar field dark energy density dominates in the early universe (see Ref. [17] for more details).

During the parameter exploration using the MCMC method, we set priors on parameters. We restrict the range of the Hubble constant to $0.2 \leq h \leq 1.0$, the reionization optical depth to $\tau \geq 0.005$, the dark energy equation of state parameter in the XCDM parameterization to $-3 \leq w \leq 0.2$, and the slope of the inverse power-law scalar field potential energy density index to $0 \leq \alpha \leq 10$ with flat priors. We also apply flat priors to other cosmological parameters, with sufficiently wide ranges so that they do not affect parameter estimation: e.g., $0.005 \leq \Omega_b h^2 \leq 0.1$, $0.001 \leq \Omega_c h^2 \leq 0.99$, $0.5 \leq 100\theta_{\text{MC}} \leq 10$, $-0.5 \leq \Omega_k \leq 0.5$, and $0.8 \leq n_s \leq 1.2$, etc.

In our analysis, we consider the contribution of photons, massless and massive neutrinos by assuming the present CMB temperature $T_0 = 2.7255$ K, the effective number of neutrino species $N_{\text{eff}} = 3.04$, and a single massive neutrino species with neutrino mass 0.06 eV.

The SPTpol data alone is not able to tightly constrain the reionization optical depth (τ) as it is not so sensitive to τ , and the τ parameter is strongly correlated with A_s . When we constrain the parameters of each model using the SPTpol data alone we use a Gaussian prior for τ , adapted from the τ value of the corresponding model constrained using the Planck 2015 CMB and the non-CMB data sets, and instead of A_s and τ we use the combination $10^9 A_s e^{-2\tau}$ as an alternative free parameter following the SPTpol team [25]. However, it should be emphasized that the resulting SPTpol parameter constraints strongly depend on the choice of the prior of τ .

We use the converged MCMC chains to present mean values, their confidence limits, and likelihood distributions of the model parameters. The convergence of the MCMC chains are checked with the Gelman and Rubin R statistic using the COSMOMC getdist routine.

IV. MODEL POWER SPECTRA

Quantum-mechanical fluctuations during inflation generate the primordial energy density spatial inhomogeneity power spectra we use in our analyses here.

An initial epoch of non-slow-roll (tilted) spatially-flat inflation is used to produce the primordial power spectrum in the spatially-flat models [28],

$$P(k) = A_s \left(\frac{k}{k_0} \right)^{n_s}, \quad (5)$$

where k is wavenumber and the pivot wavenumber $k_0 = 0.05 \text{ Mpc}^{-1}$. This model and power spectrum expression remain valid in the slow-roll limit where $n_s = 1$ and they are untilted. An initial epoch of slow-roll (untilted) non-flat inflation is used to produce the power spectrum in the non-flat models [29–32],

$$P(q) \propto \frac{(q^2 - 4K)^2}{q(q^2 - K)}, \quad (6)$$

where $q = \sqrt{k^2 + K}$ is the non-flat space wavenumber and $K = -(H_0^2/c^2)\Omega_k$ is the spatial curvature. In the negative Ω_k closed model, the eigenvalue of the spatial Laplacian is $\propto -(q^2 - K)/K \equiv -\bar{k}^2/K$ and the normal modes are labeled by $qK^{-1/2} = 3, 4, 5, \dots$. In the non-flat models this $P(q)$ is normalized to A_s at the k_0 pivot wavenumber. In the spatially-flat $K = 0$ limit this $P(q)$ reduces to the untilted $n_s = 1$ power spectrum. Unlike in the flat case, in the non-flat case it has not yet been possible to determine the power spectrum in a non-slow-roll inflation model.

On the other hand, the Planck non-flat model analyses [2, 3] do not make use of either of the above power spectra. They instead use

$$P_{\text{Planck}}(q) \propto \frac{(q^2 - 4K)^2}{q(q^2 - K)} \left(\frac{\bar{k}}{k_0} \right)^{n_s-1}, \quad (7)$$

where besides using the non-flat space wavenumber q , the wavenumber \bar{k} is also used to define (and tilt) the non-flat model $P(q)$. The \bar{k}^{n_s-1} tilt factor in $P_{\text{Planck}}(q)$ is based on the assumption that tilt in a non-flat model works somewhat like it does in a flat model. This does not seem likely given that spatial curvature introduces an additional length scale in the non-flat case (i.e., in addition to the Hubble length). It is not known if the primordial power spectrum of Eq. (7) is the consequence of quantum fluctuations during an epoch of inflation. However, this power spectrum is physically consistent if $n_s = 1$ or if $K = 0$, when it reduces to the power spectrum of Eqs. (6) or (5), both of which are consequences of quantum fluctuations during inflation.

V. OBSERVATIONAL CONSTRAINTS

The cosmological parameter constraints we describe in what follows were derived using the inflation power spectrum of Eq. (5) in the spatially-flat models and Eq. (6) in the non-flat models. In both cases we consider three different dark energy models, a time-independent cosmological constant and dynamical X -fluid and scalar field dark energy densities.

Figures 1–3 show the likelihood distributions of model parameters of the tilted flat ΛCDM , XCDM , and ϕCDM models derived by using the SPTpol-TE, SPTpol-EE, and SPTpol-TE+EE data. As mentioned above, we use the combination $10^9 A_s e^{-2\tau}$ as a free parameter. In addition to the other four or five free cosmological parameters that characterize these models, these plots also show constraints on three derived cosmological parameters, namely, H_0 , the current matter density parameter (Ω_m), and the current amplitude of mass fluctuation at $8 \text{ h}^{-1}\text{Mpc}$ scale (σ_8). In each figure, the result from the joint analysis of Planck CMB data (TT+lowP+lensing) and non-CMB data sets is shown for comparison. We note that our results for the SPTpol-TE+EE data are very similar to those of Ref. [25].

Table II lists mean values and 68.3% confidence ranges of cosmological parameters of the tilted flat ΛCDM , XCDM , and ϕCDM models constrained using the SPTpol TE+EE, TE, and EE data sets. We note that a different Gaussian prior of reionization optical depth that best-fits the Planck CMB and non-CMB data has been applied for each dark energy model.

In the tilted flat XCDM and ϕCDM models, the dark energy parameters (w and α), H_0 , and Ω_m are not tightly constrained by the SPTpol data alone. The SPTpol data (TE+EE and EE) prefer a larger value of H_0 in the ΛCDM model (as found in Ref. [25]) and lower values of H_0 in both dynamical dark energy models, and particularly in the ϕCDM model the estimated SPTpol Hubble constant is significantly lower than the best-fit value obtained using the Planck CMB and non-CMB data. However, we note that in the XCDM model high values of Hubble constant near the upper bound of the prior are

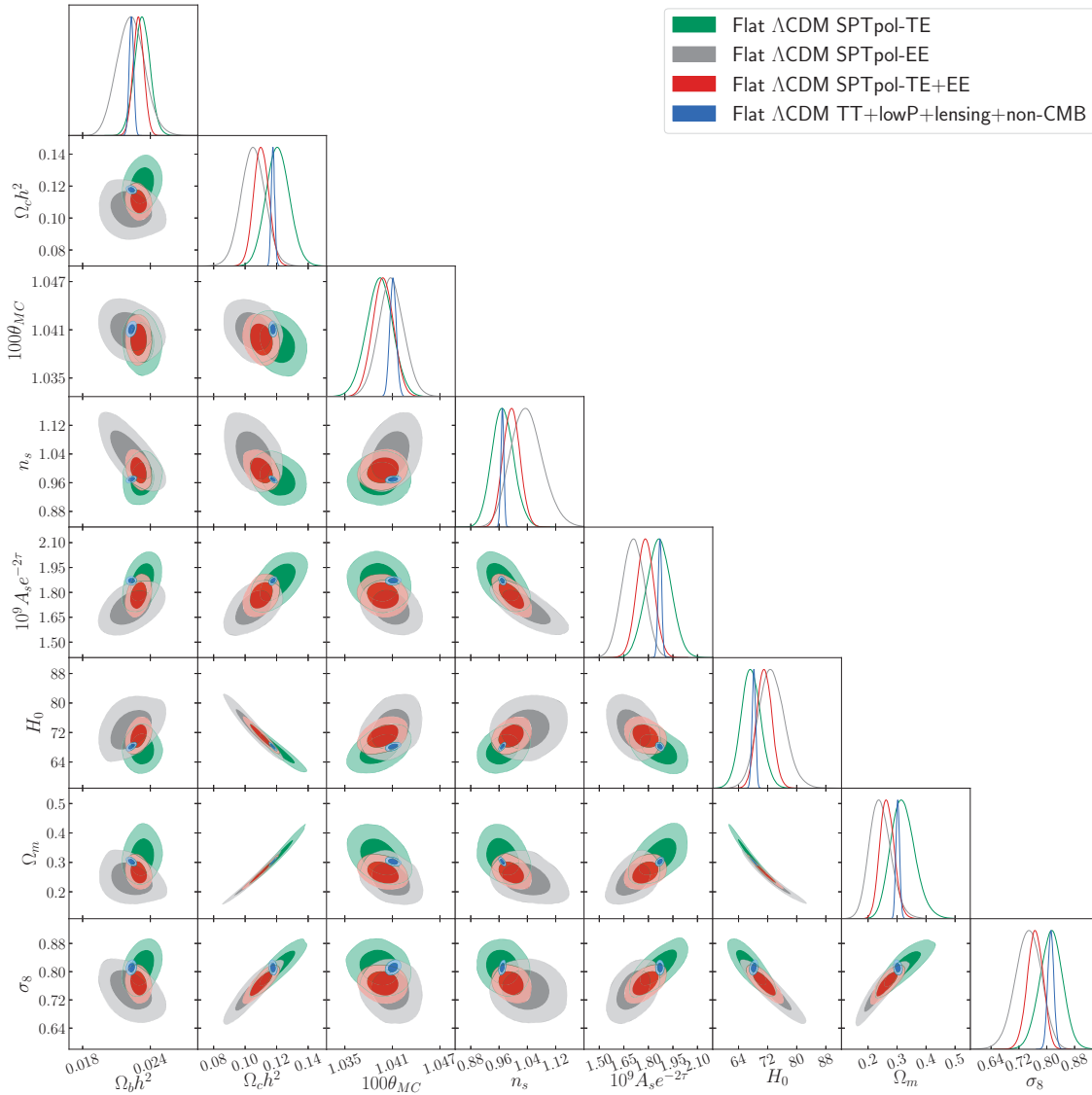


FIG. 1: Likelihood distributions of the tilted flat Λ CDM model parameters constrained by using the SPTpol TE, EE, and TE+EE data. For comparison, results from the Planck 2015 data (TT+lowP+lensing) together with non-CMB data sets (BAO, SN, $H(z)$, $f\sigma_8$) are also shown. The red contours here are very similar to the equivalent grey contours in Fig. 12 of Ref. [25].

allowed and there are strong degeneracies between the Hubble constant and w , Ω_m , and σ_8 : w and Ω_m have negative correlation with H_0 while σ_8 has positive correlation. In the tilted flat ϕ CDM model, the SPTpol data alone do not constrain α , allowing larger values of α exceeding the upper bound of the prior ($\alpha < 10$). Larger values of α correspond to smaller values of the Hubble constant. The ϕ CDM model SPTpol Hubble constant has similar correlations with Ω_m and σ_8 , as in the XCDM parameterization case.

Figures 4–6 show the likelihood distributions of the tilted flat Λ CDM, XCDM, and ϕ CDM model parameters constrained using different combinations of Planck 2015 CMB (TT+lowP+lensing), SPTpol, and non-CMB data. Here we do not apply a Gaussian prior on τ since the

Planck CMB data provide a tight constraint on this parameter, but the combined parameter $10^9 A_s e^{-2\tau}$ is still used for comparison with the previous figures. We see that the combination of Planck and SPTpol CMB data (TT+lowP+lensing+SPTpol-TE+EE) is unable to place tight constraints on the dark energy parameters (w and α), H_0 , Ω_m , and σ_8 in the XCDM and ϕ CDM dynamical dark energy models.

From our previous analysis of the CMB and non-CMB data [13, 17], we note that, in conjunction with Planck data, BAO data are the most powerful in constraining these parameters. Without the Planck CMB data sets, however, the BAO data alone (or combined with other non-CMB data) cannot give tight constraints on model parameters. Let us compare the case of SPTpol TE+EE

TABLE II: Tilted flat Λ CDM, XCDM, and ϕ CDM model parameters constrained by using SPTpol TE+EE, TE, and EE data (mean and 68.3% confidence limits).

Tilted flat Λ CDM ($\tau = 0.066 \pm 0.012$ [13])				
Parameter	SPTpol TE+EE	SPTpol TE	SPTpol EE	TT+lowP+lensing+Non-CMB
$\Omega_b h^2$	0.02295 ± 0.00048	0.02328 ± 0.00071	0.0223 ± 0.0012	0.02232 ± 0.00019
$\Omega_c h^2$	0.1103 ± 0.0048	0.1208 ± 0.0074	0.1051 ± 0.0076	0.1177 ± 0.0011
$100\theta_{\text{MC}}$	1.0398 ± 0.0013	1.0394 ± 0.0016	1.0409 ± 0.0016	1.04108 ± 0.00041
$10^9 A_s e^{-2\tau}$	1.782 ± 0.053	1.863 ± 0.075	1.707 ± 0.068	1.871 ± 0.011
n_s	0.995 ± 0.024	0.971 ± 0.031	1.038 ± 0.045	0.9692 ± 0.0043
H_0 [km s $^{-1}$ Mpc $^{-1}$]	71.1 ± 2.1	67.4 ± 2.7	73.1 ± 3.7	68.19 ± 0.50
Ω_m	0.266 ± 0.025	0.321 ± 0.042	0.243 ± 0.038	0.3025 ± 0.0064
σ_8	0.767 ± 0.023	0.812 ± 0.033	0.747 ± 0.038	0.8117 ± 0.0088
Tilted flat XCDM ($\tau = 0.068 \pm 0.015$ [13])				
Parameter	SPTpol TE+EE	SPTpol TE	SPTpol EE	TT+lowP+lensing+Non-CMB
$\Omega_b h^2$	0.02282 ± 0.00049	0.02261 ± 0.00095	0.0222 ± 0.0012	0.02233 ± 0.00021
$\Omega_c h^2$	0.1146 ± 0.0077	0.130 ± 0.013	0.1097 ± 0.0096	0.1175 ± 0.0014
$100\theta_{\text{MC}}$	1.0395 ± 0.0013	1.0388 ± 0.0017	1.0406 ± 0.0016	1.04108 ± 0.00042
$10^9 A_s e^{-2\tau}$	1.800 ± 0.059	1.862 ± 0.077	1.738 ± 0.077	1.870 ± 0.012
n_s	0.983 ± 0.029	0.940 ± 0.044	1.026 ± 0.047	0.9696 ± 0.0051
w	-0.70 ± 0.44	-0.54 ± 0.57	-0.74 ± 0.44	-0.994 ± 0.033
H_0 [km s $^{-1}$ Mpc $^{-1}$]	62 ± 15	56 ± 15	64 ± 16	68.06 ± 0.77
Ω_m	0.42 ± 0.18	0.57 ± 0.24	0.38 ± 0.19	0.3034 ± 0.0073
σ_8	0.68 ± 0.13	0.66 ± 0.19	0.68 ± 0.14	0.810 ± 0.011
Tilted flat ϕ CDM ($\tau = 0.074 \pm 0.014$ [17])				
Parameter	SPTpol TE+EE	SPTpol TE	SPTpol EE	TT+lowP+lensing+Non-CMB
$\Omega_b h^2$	0.02280 ± 0.00048	0.02282 ± 0.00075	0.0222 ± 0.0012	0.02238 ± 0.00020
$\Omega_c h^2$	0.1164 ± 0.0061	0.1246 ± 0.0082	0.1124 ± 0.0086	0.1168 ± 0.0013
H_0 [km s $^{-1}$ Mpc $^{-1}$]	52.0 ± 5.6	51.3 ± 5.9	52.4 ± 6.2	67.63 ± 0.62
$10^9 A_s e^{-2\tau}$	1.810 ± 0.055	1.859 ± 0.076	1.756 ± 0.072	1.867 ± 0.011
n_s	0.977 ± 0.026	0.952 ± 0.034	1.017 ± 0.044	0.9715 ± 0.0045
α [95.4% C.L.]	< 9.6	< 9.8	< 9.7	< 0.22
$100\theta_{\text{MC}}$	1.0392 ± 0.0013	1.0390 ± 0.0016	1.0402 ± 0.0016	1.04101 ± 0.00042
Ω_m	0.54 ± 0.11	0.58 ± 0.12	0.51 ± 0.12	0.3059 ± 0.0068
σ_8	0.599 ± 0.061	0.636 ± 0.078	0.581 ± 0.068	0.8055 ± 0.0098

Note: Parameter constraints for Planck 2015 TT+lowP+lensing and non-CMB (SN, BAO, $H(z)$, $f\sigma_8$) data sets are from Ref. [13] for the Λ CDM and XCDM models and Ref. [17] for the ϕ CDM model. For the SPTpol analyses, a different Gaussian prior for τ (indicated in the subheadings) has been used for each cosmological model (see main text for discussion and details).

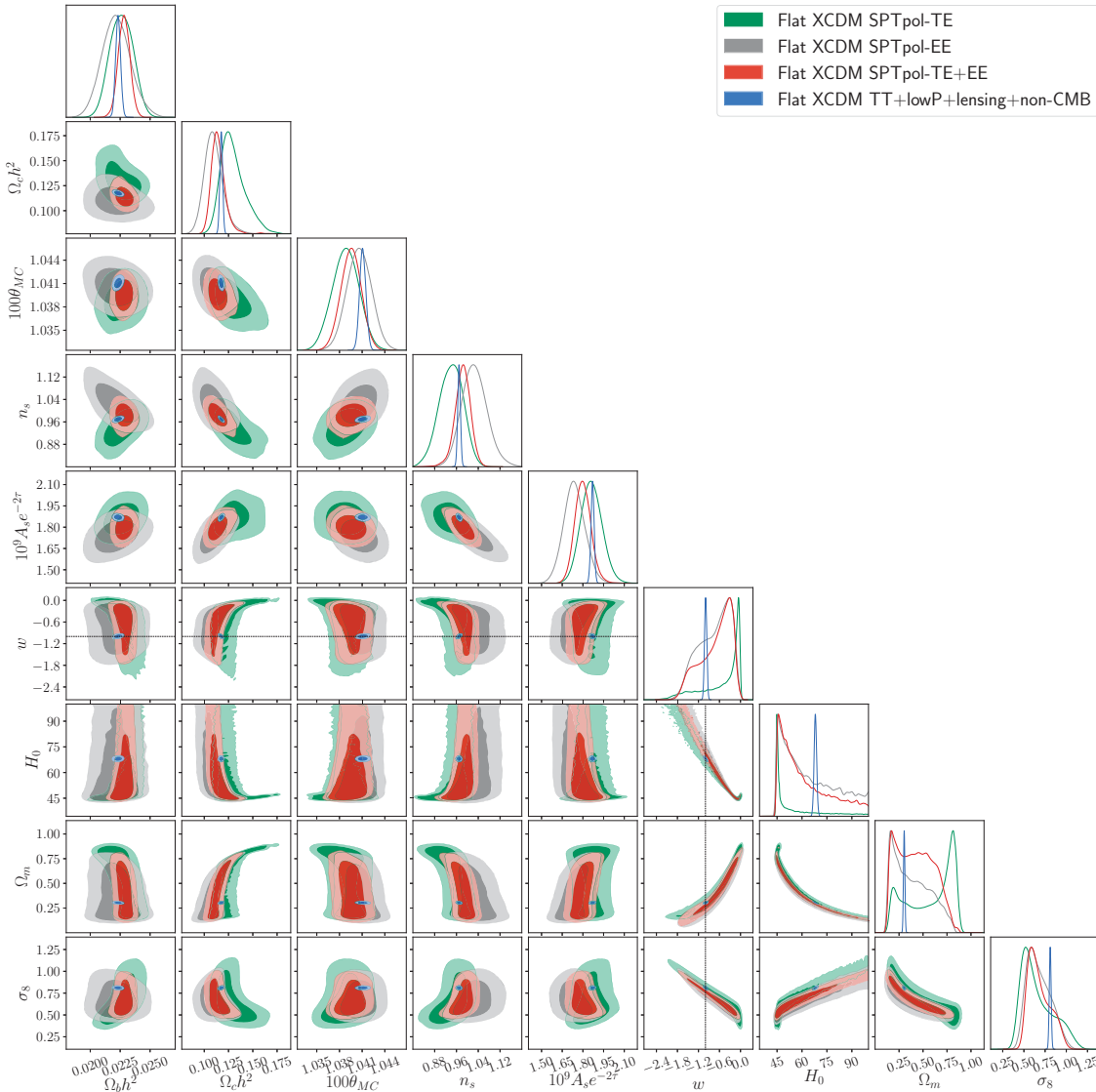


FIG. 2: Likelihood distributions of the tilted flat XCDM model parameters constrained by using the SPTpol TE, EE, and TE+EE data. For comparison, results from the Planck 2015 data (TT+lowP+lensing) together with non-CMB data sets (BAO, SN, $H(z)$, $f\sigma_8$) are also shown. Dotted straight lines indicate $w = -1$.

data alone and the case of the SN+BAO+ $H(z)$ data combination whose results are shown in Ref. [33]. Both in the flat and the nonflat dark energy models, the SPTpol TE+EE data better constrains $\Omega_b h^2$, $\Omega_c h^2$, and Ω_k (for nonflat models) while the SN+BAO+ $H(z)$ is better for the Hubble constant (H_0) and dark energy parameters w and α (for XCDM and ϕ CDM models) (see Table 2 of Ref. [33] and Tables II and V of this paper). Thus, we cannot say that the statistical weight of the SPTpol data is lower than that of the BAO data.

Comparing the cases of TT+lowP+lensing+non-CMB and TT+lowP+lensing+non-CMB+SPTpol-TE+EE, we see that the non-CMB data are significantly better at helping constrain cosmological model parameters than are the SPTpol-TE+EE data, particularly in XCDM and

ϕ CDM models. A summary of cosmological parameter values estimated from the three different combination of data sets is given in Table III. From this table and the figures, we see that, in the case of the tilted flat dark energy models, the main effects of adding the SPTpol TE+EE data to the TT+lowP+lensing+non-CMB data are a very slight tightening of the constraints on $\Omega_b h^2$ and θ_{MC} .

We now examine the consistency between the tilted flat Λ CDM, XCDM, and ϕ CDM model constraints determined from the SPTpol data and those determined from the Planck CMB and the non-CMB data sets. Following Ref. [3] we quantify the consistency between the two sets of constraints by using the statistics of χ^2 's for

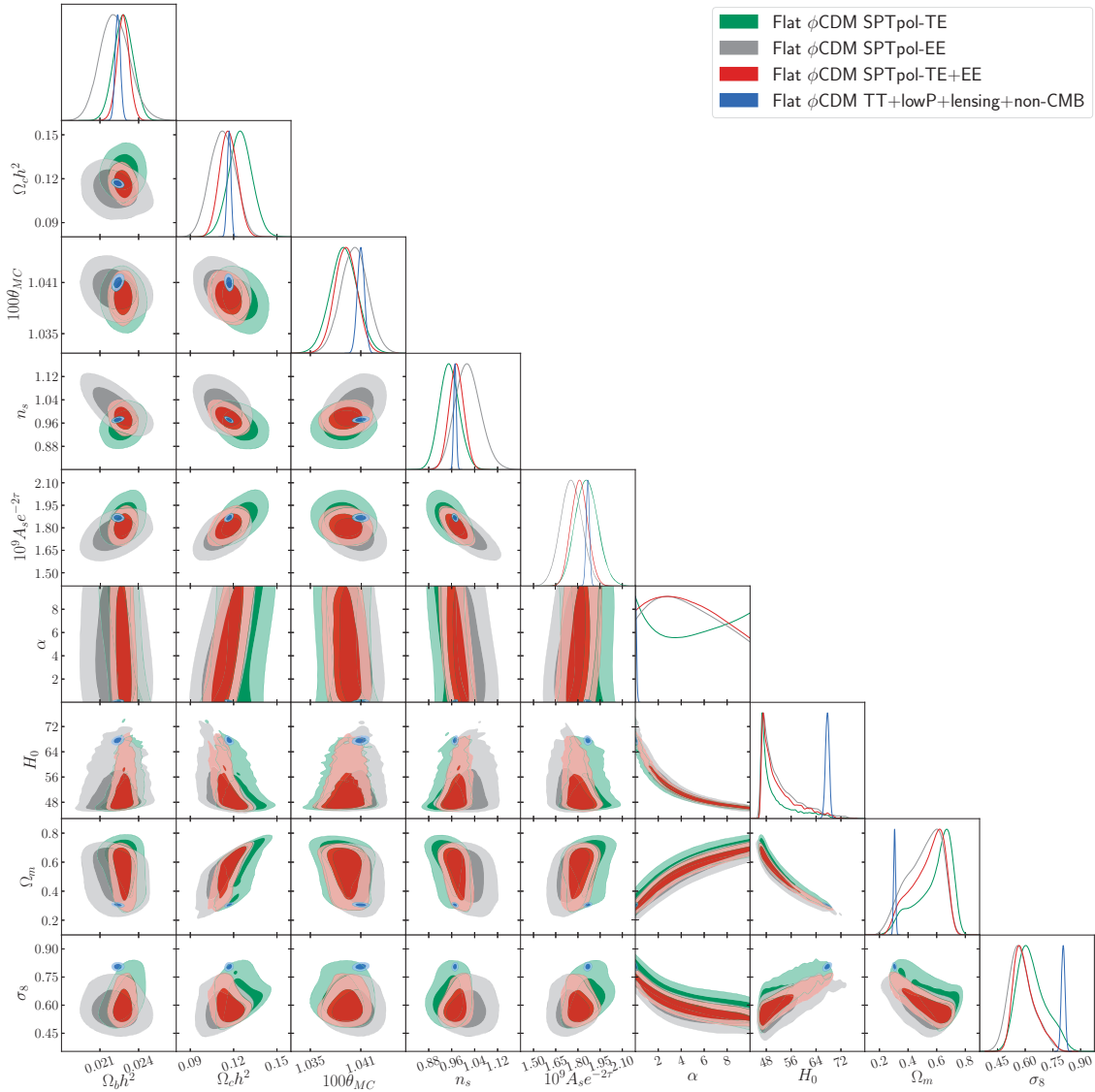


FIG. 3: Likelihood distributions of the tilted flat ϕ CDM model parameters constrained by using the SPTpol TE, EE, and TE+EE data. For comparison, results from the Planck 2015 data (TT+lowP+lensing) together with non-CMB data sets (BAO, SN, $H(z)$, $f\sigma_8$) are also shown. In the ϕ CDM model, H_0 is used as an active free parameter instead of $100\theta_{MC}$, but $100\theta_{MC}$ is shown here above H_0 for ease of comparison with other figures.

the parameter differences,

$$\chi_p^2 = \Delta\mathbf{p}^T \mathbf{C}_p^{-1} \Delta\mathbf{p}, \quad (8)$$

where \mathbf{C}_p is the covariance matrix of cosmological parameters constrained by the SPTpol data alone and $\Delta\mathbf{p}$ denotes the difference between the mean model parameters estimated from the SPTpol data and the best-fit ones estimated from the Planck 2015 CMB and non-CMB data. Following the Planck 2018 team's analysis [3], the small errors of parameters determined from the Planck CMB and non-CMB data are neglected.

From the χ^2 distribution with k degrees of freedom, we compute the probability to exceed (PTE),

$$\text{PTE} = 1 - P(k/2, \chi_p^2/2) \quad (9)$$

where $P(a, x) \equiv \gamma(a, x)/\Gamma(a)$ with the lower incomplete gamma function $\gamma(a, x) = \int_0^x e^{-t} t^{a-1} dt$ and the ordinary gamma function $\Gamma(a) = \gamma(a, \infty)$. The probability for exceeding the computed χ_p^2 is estimated from the χ^2 distribution with a given number of degrees of freedom (k), which is 5 for the tilted flat Λ CDM model and 6 for the tilted flat XCDM and ϕ CDM models. The results for the tilted flat Λ CDM, XCDM, and ϕ CDM models are summarized in the last two columns of Table IV. Here N_b is the number of band powers of each SPTpol spectrum data set, χ_{\min}^2 denotes the minimum χ^2 value for the particular data and model, and $N_\sigma = (\chi_{\min}^2 - N_{\text{dof}})/\sqrt{2N_{\text{dof}}}$ indicates the deviation of χ_{\min}^2 from the expected value $\langle \chi_{\min}^2 \rangle = N_{\text{dof}}$. The number of degrees of freedom N_{dof}

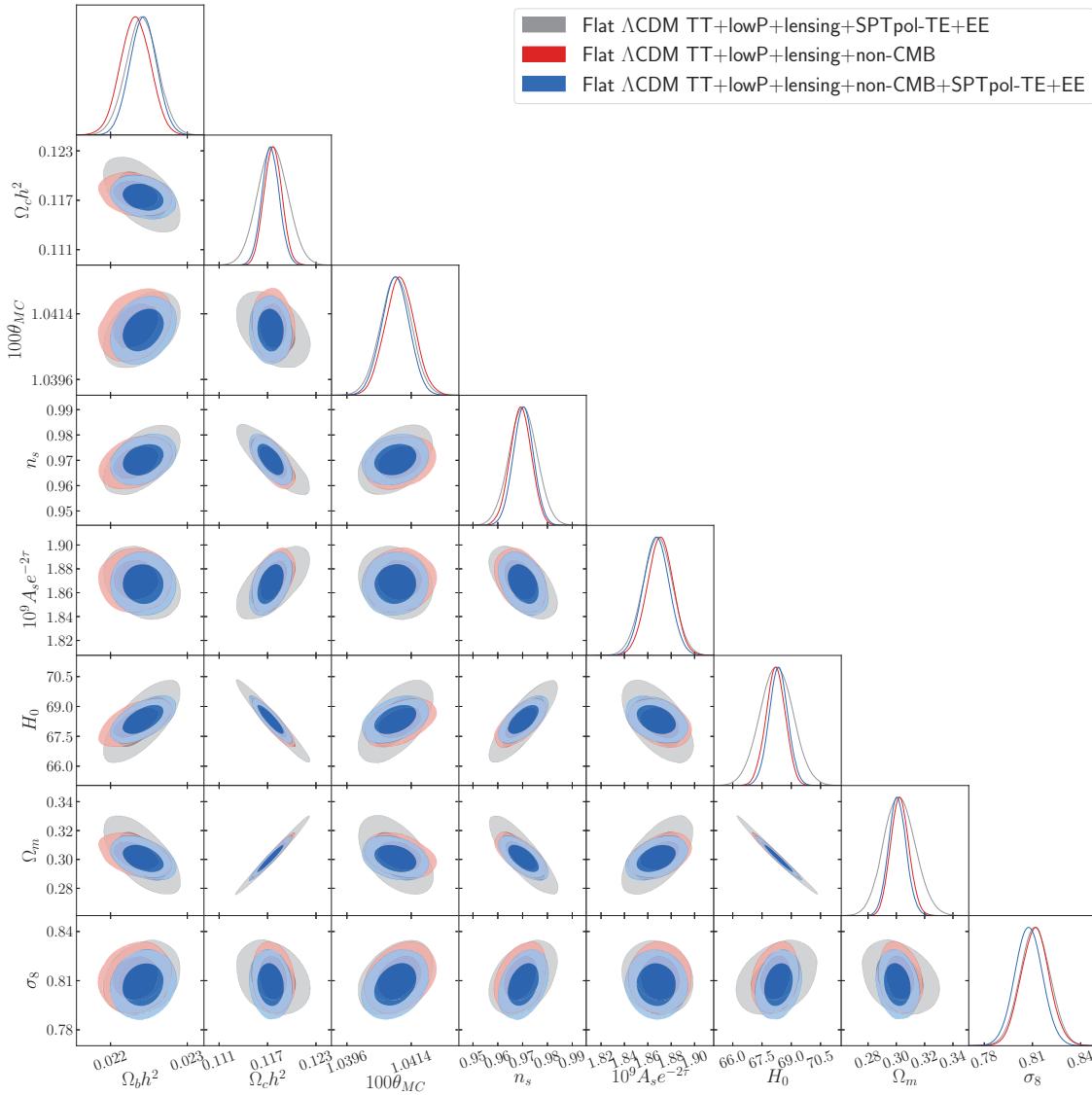


FIG. 4: Likelihood distributions of the tilted flat Λ CDM model parameters constrained by using the Planck 2015 TT+lowP+lensing data in conjunction with SPTpol TE+EE and non-CMB data.

is given by the number of data band powers minus the number of cosmological parameters (five for the Λ CDM and six for the XCDM and ϕ CDM models) and three nuisance parameters: $N_{\text{dof}} = N_b - 8$ for the Λ CDM model and $N_{\text{dof}} = N_b - 9$ for the XCDM and ϕ CDM models (see Ref. [3] for a detailed description).

The χ^2_{min} for the best-fit Planck 2018 cosmology or the best-fit Λ CDM, XCDM, and ϕ CDM models constrained by using the Planck 2015 CMB and non-CMB data is the minimum χ^2 value and has been obtained by varying the SPTpol data-related nuisance and foreground parameters while fixing the best-fit cosmological parameters of the corresponding model. On the other hand, the χ^2_{min} for the SPTpol data has been obtained by varying all the cosmological, nuisance, and foreground parameters. Powell's minimization method (implemented

in the COSMOMC program) has been used to find the best-fit model and the minimum value of the χ^2 . χ^2_{min} and N_σ for the fits of the best-fit Planck 2018 tilted flat Λ CDM model and the best-fit TT+lowP+lensing+non-CMB tilted flat models to the SPTpol data are shown in the third and fourth columns of Table IV, while the corresponding numbers for the fits of the best-fit SPTpol tilted flat models to the SPTpol data are listed in the fifth and sixth columns of this table.

Our results for the Planck 2018 best-fit flat Λ CDM model and the SPTpol best-fit flat Λ CDM model with the Gaussian prior on τ used in [25] are similar to those presented in the Planck 2018 analysis (Table 3 of Ref. [3]). The values of χ^2_{min} and N_σ for the Planck 2018 best-fit cosmology are higher than those for the best-fit Λ CDM model constrained with SPTpol data, which sug-

TABLE III: Tilted flat Λ CDM, XCDM, and ϕ CDM model parameters constrained by using Planck 2015, SPTpol TE+EE, and non-CMB data (mean and 68.3% confidence limits).

Tilted flat Λ CDM			
Parameter	TT+lowP+lensing+SPTpol	TT+lowP+lensing+non-CMB	TT+lowP+lensing+non-CMB+SPTpol
$\Omega_b h^2$	0.02241 ± 0.00020	0.02232 ± 0.00019	0.02243 ± 0.00018
$\Omega_c h^2$	0.1176 ± 0.0019	0.1177 ± 0.0011	0.1174 ± 0.0011
$100\theta_{\text{MC}}$	1.04097 ± 0.00043	1.04108 ± 0.00041	1.04096 ± 0.00038
τ	0.067 ± 0.016	0.066 ± 0.012	0.064 ± 0.012
$\ln(10^{10} A_s)$	3.062 ± 0.029	3.061 ± 0.023	3.054 ± 0.023
n_s	0.9702 ± 0.0056	0.9692 ± 0.0043	0.9703 ± 0.0041
$10^9 A_s e^{-2\tau}$	1.868 ± 0.013	1.871 ± 0.011	1.867 ± 0.011
$H_0 [\text{km s}^{-1} \text{ Mpc}^{-1}]$	68.24 ± 0.85	68.19 ± 0.50	68.34 ± 0.48
Ω_m	0.302 ± 0.011	0.3025 ± 0.0064	0.3008 ± 0.0062
σ_8	0.8117 ± 0.0093	0.8117 ± 0.0088	0.8076 ± 0.0087
Tilted flat XCDM			
Parameter	TT+lowP+lensing+SPTpol	TT+lowP+lensing+non-CMB	TT+lowP+lensing+non-CMB+SPTpol
$\Omega_b h^2$	0.02243 ± 0.00020	0.02233 ± 0.00021	0.02245 ± 0.00019
$\Omega_c h^2$	0.1175 ± 0.0019	0.1175 ± 0.0014	0.1171 ± 0.0014
$100\theta_{\text{MC}}$	1.04102 ± 0.00043	1.04108 ± 0.00042	1.04099 ± 0.00040
τ	0.060 ± 0.017	0.068 ± 0.015	0.066 ± 0.015
$\ln(10^{10} A_s)$	3.049 ± 0.031	3.063 ± 0.027	3.059 ± 0.027
n_s	0.9705 ± 0.0056	0.9696 ± 0.0051	0.9711 ± 0.0047
w	-1.37 ± 0.32	-0.994 ± 0.033	-0.989 ± 0.032
$10^9 A_s e^{-2\tau}$	1.868 ± 0.013	1.870 ± 0.012	1.867 ± 0.011
$H_0 [\text{km s}^{-1} \text{ Mpc}^{-1}]$	81 ± 11	68.06 ± 0.77	68.10 ± 0.76
Ω_m	0.226 ± 0.067	0.3034 ± 0.0073	0.3024 ± 0.0071
σ_8	0.911 ± 0.085	0.810 ± 0.011	0.805 ± 0.011
Tilted flat ϕ CDM			
Parameter	TT+lowP+lensing+SPTpol	TT+lowP+lensing+non-CMB	TT+lowP+lensing+non-CMB+SPTpol
$\Omega_b h^2$	0.02237 ± 0.00021	0.02238 ± 0.00020	0.02250 ± 0.00018
$\Omega_c h^2$	0.1182 ± 0.0019	0.1168 ± 0.0013	0.1165 ± 0.0013
$H_0 [\text{km s}^{-1} \text{ Mpc}^{-1}]$	63.3 ± 3.4	67.63 ± 0.62	67.76 ± 0.62
τ	0.072 ± 0.016	0.074 ± 0.014	0.072 ± 0.014
$\ln(10^{10} A_s)$	3.074 ± 0.030	3.074 ± 0.025	3.069 ± 0.025
n_s	0.9690 ± 0.0057	0.9715 ± 0.0045	0.9726 ± 0.0045
α [95.4% C.L.]	< 1.62	< 0.22	< 0.22
$10^9 A_s e^{-2\tau}$	1.872 ± 0.012	1.867 ± 0.011	1.864 ± 0.011
$100\theta_{\text{MC}}$	1.04070 ± 0.00044	1.04101 ± 0.00042	1.04090 ± 0.00039
Ω_m	0.355 ± 0.042	0.3059 ± 0.0068	0.3043 ± 0.0067
σ_8	0.770 ± 0.030	0.8055 ± 0.0098	0.8016 ± 0.0096

Note: Parameter constraints for Planck 2015 TT+lowP+lensing and non-CMB (SN, BAO, $H(z)$, $f\sigma_8$) data sets are from Ref. [13] for the Λ CDM and XCDM models and Ref. [17] for the ϕ CDM model.

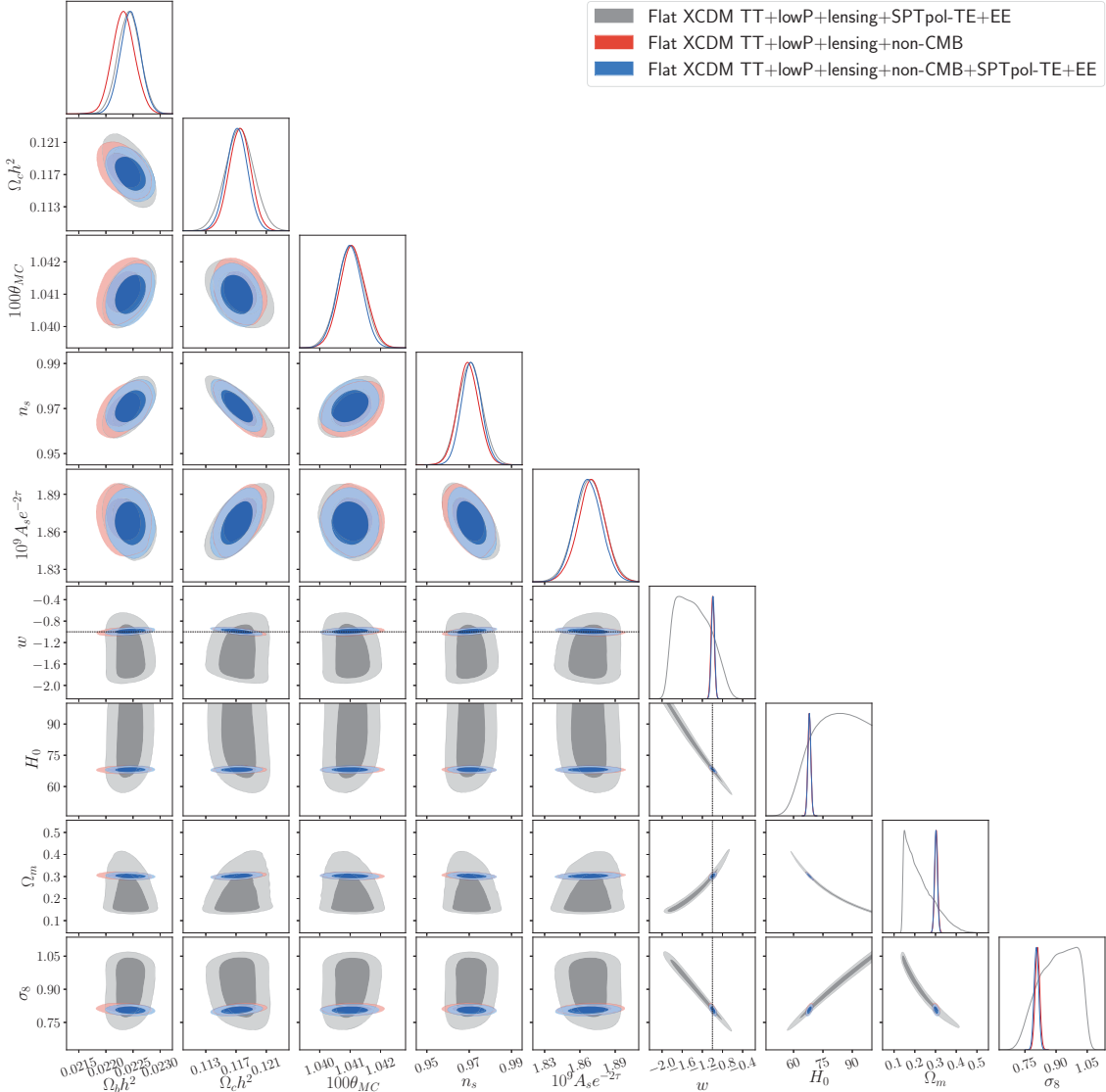


FIG. 5: Likelihood distributions of the tilted flat XCDM model parameters constrained by using the Planck 2015 TT+lowP+lensing data in conjunction with SPTpol TE+EE and non-CMB data. Dotted straight lines indicate $w = -1$.

gests that the SPTpol data disfavor the Λ CDM cosmology that best-fits the Planck 2018 data. The same holds for the best-fit tilted flat Λ CDM, XCDM, and ϕ CDM models as shown in Table IV. We note that in all cases of SPTpol TE+EE N_σ is larger than 2.2 so the best-fit models do not provide good fits to the SPTpol TE+EE data. The XCDM model fits the SPTpol TE+EE, TE, and EE data sets better than does the Λ CDM model. Here $\chi^2_{\min} = 62.36$ for the best-fit flat XCDM model favored by the SPTpol TE data is at least 5 less than the values of the best-fit Λ CDM and ϕ CDM models. The ϕ CDM model with larger χ^2_{\min} and N_σ poorly fits the SPTpol data.

Comparing χ^2_p values in the tilted flat Λ CDM, XCDM, and ϕ CDM models implies there is a discrepancy between the best-fit model favored by the Planck CMB and non-

CMB data and that favored by the SPTpol data alone. For the SPTpol TE+EE data, the discrepancy in the XCDM case is smaller than that in the Λ CDM model. The ϕ CDM model has an even bigger discrepancy than the other two models, with larger χ^2_p and smaller PTE value, [34]. However, there is no significant evidence of tension between the ϕ CDM (or Λ CDM or XCDM) model constrained using the Planck CMB and non-CMB data and that constrained using SPTpol data alone (as can be seen in the last column of Table IV).

We now consider the untilted non-flat model constraints derived using the SPTpol data alone. Figures 7–9 show the likelihood distributions of model parameters of the untilted non-flat Λ CDM, XCDM, and ϕ CDM models that are favored by the SPTpol data sets. In each figure, the joint analysis results obtained by us-

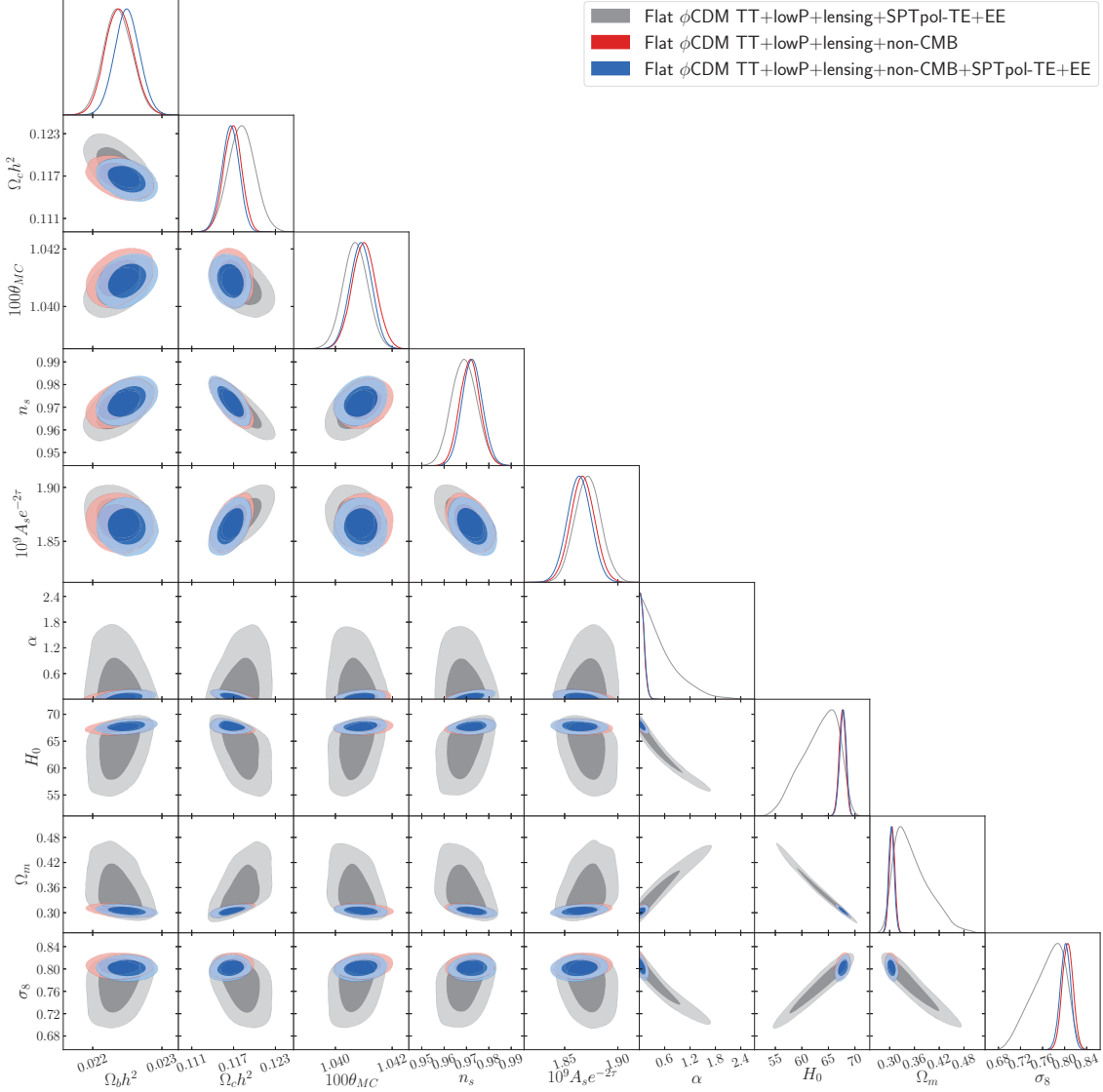


FIG. 6: Likelihood distributions of the tilted flat ϕ CDM model parameters constrained by using the Planck 2015 TT+lowP+lensing data in conjunction with SPTpol TE+EE and non-CMB data.

ing the Planck 2015 CMB and non-CMB data are also shown. Compared to the combination of the Planck CMB and non-CMB data, the SPTpol data sets tend to prefer smaller values of θ_{MC} . As in the tilted flat models with SPTpol data, the observations prefer a parameter space where the Hubble constant is anti-correlated with the matter density Ω_m and has some degeneracy with the curvature parameter Ω_k .

The mean values and 68.3% confidence ranges of the cosmological parameters of untilted non-flat dark energy models are summarized in Table V. In the untilted non-flat Λ CDM model, the SPTpol data favor a larger Hubble constant value while the situation is the opposite in the XCDM and ϕ CDM models. The SPTpol data by itself does not significantly constrain the spatial curvature parameter Ω_k .

Figures 10–12 show the likelihood distributions of the untilted non-flat Λ CDM, XCDM, and ϕ CDM model parameters constrained using different combinations of Planck 2015 CMB (TT+lowP+lensing), SPTpol, and non-CMB data sets. Again, we do not use a Gaussian prior on τ in these analyses since the Planck CMB data provide a tight constraint on this parameter. We see that the combination of Planck and SPTpol data (TT+lowP+lensing+SPTpol-TE+EE) is unable to place tight constraints on the dark energy parameters (w and α), H_0 , Ω_k , Ω_m , and σ_8 in all three models. The degeneracies between parameters seen in the constraints from the SPTpol data alone are also present here. Comparing the cases of TT+lowP+lensing+non-CMB and TT+lowP+lensing+non-CMB+SPTpol-TE+EE, we again find that the non-CMB data are significantly better.

TABLE IV: Minimum χ^2 values for the SPTpol TE+EE, TE, and EE spectra in the best-fit tilted flat Planck 2018 Λ CDM model, and in the best-fit tilted flat Λ CDM, XCDM, and ϕ CDM models constrained using Planck 2015 TT+lowP+SN+BAO+ $H(z)+f\sigma_8$ data [13, 17].

SPTpol spectrum	N_b	Planck 2018 cosmology [3]		SPT (Λ CDM τ [25])			
		χ^2_{\min}	N_σ	χ^2_{\min}	N_σ	χ^2_p	PTE
TE + EE	112	146.80	2.97	137.27	2.31	9.95	0.077
TE	56	71.62	2.41	68.21	2.06	3.26	0.659
EE	56	67.34	1.97	60.88	1.31	8.74	0.120
Best-fit tilted flat Λ CDM				SPT (Λ CDM τ [13])			
SPTpol spectrum	N_b	χ^2_{\min}	N_σ	χ^2_{\min}	N_σ	χ^2_p	PTE
TE + EE	112	146.84	2.97	136.92	2.28	8.41	0.135
TE	56	72.22	2.47	67.94	2.04	3.75	0.586
EE	56	67.34	1.97	60.64	1.29	7.80	0.168
Best-fit tilted flat XCDM				SPT (XCDM τ [13])			
SPTpol spectrum	N_b	χ^2_{\min}	N_σ	χ^2_{\min}	N_σ	χ^2_p	PTE
TE + EE	112	146.69	3.04	135.31	2.25	6.75	0.345
TE	56	72.17	2.60	62.36	1.58	4.08	0.666
EE	56	67.27	2.09	59.03	1.24	6.01	0.422
Best-fit tilted flat ϕ CDM				SPT (ϕ CDM τ [17])			
SPTpol spectrum	N_b	χ^2_{\min}	N_σ	χ^2_{\min}	N_σ	χ^2_p	PTE (H_0)
TE + EE	112	146.59	3.04	139.27	2.53	21.85	0.001
TE	56	72.14	2.59	68.21	2.19	15.68	0.016
EE	56	67.29	2.09	61.28	1.47	17.50	0.008
SPTpol spectrum	N_b	χ^2_{\min}	N_σ	χ^2_{\min}	N_σ	χ^2_p	PTE (θ_{MC})
TE + EE	112	146.59	3.04	139.27	2.53	10.84	0.093
TE	56	72.14	2.59	68.21	2.19	6.18	0.403
EE	56	67.29	2.09	61.28	1.47	9.99	0.125

Note: We assume a different Gaussian prior of τ for each cosmological model. For the best-fit tilted flat Planck 2018 model, and the best-fit tilted flat Λ CDM, XCDM, and ϕ CDM models constrained using Planck 2015 and non-CMB data, we apply $\tau = 0.078 \pm 0.019$ [25], 0.066 ± 0.012 , 0.068 ± 0.015 [13], and 0.074 ± 0.014 [17], respectively.

ter at helping constrain cosmological model parameters than are the SPTpol-TE+EE data.

A summary of cosmological parameter values estimated from the three different combination of data sets is given in Table VI. From this table and the figures, we see that, in the case of the untilted non-flat dark energy models, the main effects of adding the SPTpol TE+EE data to the TT+lowP+lensing+non-CMB data are a very slight tightening of the constraints on θ_{MC} and Ω_bh^2 .

It is particularly interesting that including the

SPTpol TE+EE data in a joint analysis with either just the Planck 2015 TT+lowP+lensing data or with the TT+lowP+lensing+non-CMB data still results in a detection of non-zero spatial curvature with the TT+lowP+lensing+SPTpol-TE+EE data favoring a closed untilted model over the corresponding untilted flat limit at between 1.0σ and 1.6σ and the TT+lowP+lensing+non-CMB+SPTpol-TE+EE data favoring a closed untilted model over the corresponding untilted flat limit at between 3.1σ and 5.0σ .

TABLE V: Untilted non-flat Λ CDM, XCDM, ϕ CDM model parameters constrained by using the SPTpol TE+EE, TE, and EE data (mean and 68.3% confidence limits).

Untilted non-flat Λ CDM ($\tau = 0.112 \pm 0.012$)				
Parameter	SPTpol TE+EE	SPTpol TE	SPTpol EE	TT+lowP+lensing+Non-CMB
$\Omega_b h^2$	0.02280 ± 0.00048	0.02354 ± 0.00084	0.02281 ± 0.00099	0.02305 ± 0.00019
$\Omega_c h^2$	0.1120 ± 0.0054	0.1185 ± 0.0078	0.1104 ± 0.0090	0.1093 ± 0.0010
$100\theta_{\text{MC}}$	1.0397 ± 0.0013	1.0395 ± 0.0016	1.0403 ± 0.0015	1.04227 ± 0.00041
$10^9 A_s e^{-2\tau}$	1.778 ± 0.042	1.835 ± 0.066	1.761 ± 0.050	1.831 ± 0.010
Ω_k	0.017 ± 0.012	-0.001 ± 0.031	0.014 ± 0.018	-0.0083 ± 0.0016
H_0 [km s $^{-1}$ Mpc $^{-1}$]	84.4 ± 8.8	73 ± 13	84 ± 11	68.01 ± 0.62
Ω_m	0.196 ± 0.043	0.30 ± 0.12	0.200 ± 0.057	0.2875 ± 0.0055
σ_8	0.817 ± 0.031	0.845 ± 0.045	0.804 ± 0.054	0.8121 ± 0.0095
Untilted non-flat XCDM ($\tau = 0.119 \pm 0.012$)				
Parameter	SPTpol TE+EE	SPTpol TE	SPTpol EE	TT+lowP+lensing+Non-CMB
$\Omega_b h^2$	0.02271 ± 0.00051	0.02323 ± 0.00098	0.0222 ± 0.0010	0.02305 ± 0.00020
$\Omega_c h^2$	0.1135 ± 0.0060	0.1199 ± 0.0082	0.117 ± 0.011	0.1092 ± 0.0010
$100\theta_{\text{MC}}$	1.0395 ± 0.0013	1.0395 ± 0.0016	1.0401 ± 0.0015	1.04227 ± 0.00042
$10^9 A_s e^{-2\tau}$	1.773 ± 0.043	1.815 ± 0.073	1.782 ± 0.054	1.832 ± 0.010
Ω_k	-0.016 ± 0.063	-0.008 ± 0.061	0.019 ± 0.061	-0.0069 ± 0.0020
w	-0.46 ± 0.33	-0.61 ± 0.50	-0.42 ± 0.28	-0.960 ± 0.032
H_0 [km s $^{-1}$ Mpc $^{-1}$]	58 ± 17	59 ± 16	60 ± 16	67.45 ± 0.75
Ω_m	0.52 ± 0.27	0.50 ± 0.25	0.47 ± 0.23	0.2923 ± 0.0066
σ_8	0.63 ± 0.12	0.70 ± 0.16	0.60 ± 0.11	0.805 ± 0.011
Untilted non-flat ϕ CDM ($\tau = 0.122 \pm 0.012$)				
Parameter	SPTpol TE+EE	SPTpol TE	SPTpol EE	TT+lowP+lensing+Non-CMB
$\Omega_b h^2$	0.02263 ± 0.00048	0.02280 ± 0.00095	0.02210 ± 0.00096	0.02304 ± 0.00020
$\Omega_c h^2$	0.1139 ± 0.0057	0.1220 ± 0.0087	0.118 ± 0.010	0.1093 ± 0.0010
H_0 [km s $^{-1}$ Mpc $^{-1}$]	57 ± 13	61 ± 15	63 ± 14	67.36 ± 0.72
$10^9 A_s e^{-2\tau}$	1.776 ± 0.039	1.790 ± 0.070	1.790 ± 0.055	1.832 ± 0.010
Ω_k	0.010 ± 0.036	0.031 ± 0.058	0.043 ± 0.049	-0.0063 ± 0.0020
α	4.3 ± 2.7	< 9.7 [95.4% C.L.]	4.8 ± 2.7	< 0.31 [95.4% C.L.]
$100\theta_{\text{MC}}$	1.0394 ± 0.0013	1.0391 ± 0.0016	1.0399 ± 0.0015	1.04210 ± 0.00041
Ω_m	0.47 ± 0.17	0.46 ± 0.19	0.41 ± 0.16	0.2931 ± 0.0064
σ_8	0.619 ± 0.075	0.63 ± 0.11	0.600 ± 0.081	0.805 ± 0.011

Note: Parameter constraints for Planck 2015 TT+lowP+lensing and non-CMB (SN, BAO, $H(z)$, $f\sigma_8$) data sets are from Ref. [13] for the Λ CDM and XCDM models and from Ref. [17] for the ϕ CDM model. For the SPTpol analyses, a different Gaussian prior for τ (indicated in the subheadings) has been used for each cosmological model (see main text for discussions and details).

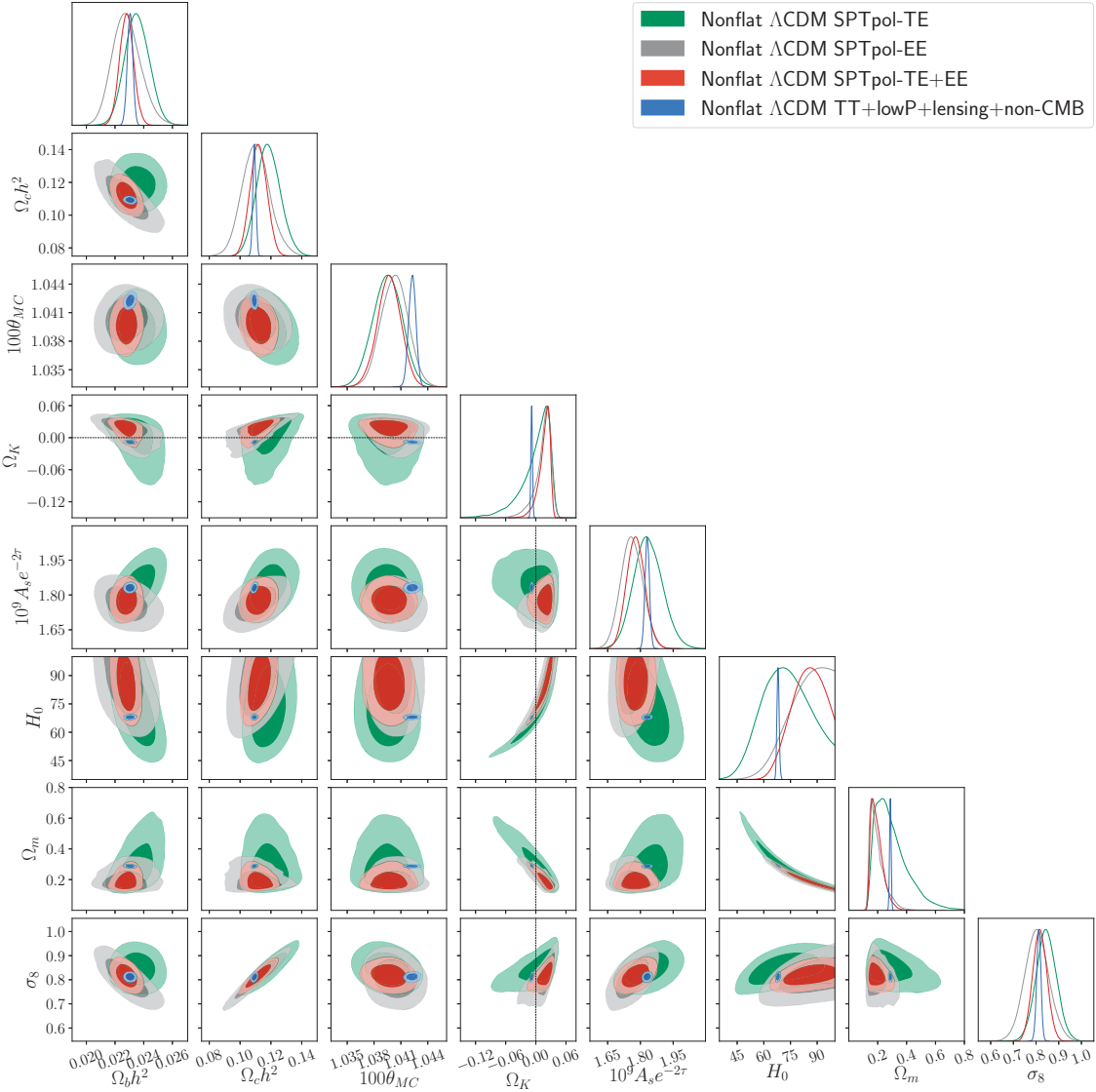


FIG. 7: Likelihood distributions of the untilted non-flat Λ CDM model parameters constrained by using the SPTpol TE+EE, TE, and EE data alone. For comparison, results from the Planck 2015 data (TT+lowP+lensing) together with non-CMB data sets (BAO, SN, $H(z)$, $f\sigma_8$) are also shown. Dotted straight lines indicate $\Omega_k = 0$.

We next examine the consistency between the untilted non-flat model constraints obtained by using the Planck CMB and non-CMB data and those determined from the SPTpol data sets. The results are summarized in Table VII. Compared to the tilted flat cases, the best-fit untilted non-flat models favored by the Planck CMB and non-CMB data have similar χ^2_{\min} and N_σ values. For the best-fit models favored by the SPTpol TE+EE and EE data, the non-flat models improve data fitting with smaller χ^2_{\min} and N_σ values than the flat models except for the case of the XCDM parameterization with SPTpol TE+EE data [37]. On the other hand, the best-fit untilted non-flat dark energy models all poorly fit the SPTpol TE data with larger χ^2_{\min} values, compared to the corresponding tilted flat models. The increase in the

χ^2_{\min} is very notable in the case of the best-fit non-flat XCDM model favored by the SPTpol TE data. For SPTpol TE+EE data, the N_σ values are all larger than 2.2 so none of the best-fit models provide a good fit to the SPTpol TE+EE data. Comparing the χ^2_p values of Table VII for the untilted non-flat Λ CDM, XCDM, and ϕ CDM models, we see that there is also no significant evidence of tension between the non-flat dark energy models constrained using the Planck CMB and non-CMB data and that constrained using SPTpol data alone.

Except for the untilted non-flat Λ CDM model where the SPTpol TE+EE data favors a σ_8 value ($\sigma_8 = 0.817 \pm 0.031$) that is 0.5σ larger than that favored by the Planck 2015 TT+lowP+lensing data ($\sigma_8 = 0.799 \pm 0.021$, [15]), the SPTpol TE+EE data favor σ_8 values between 1.1σ

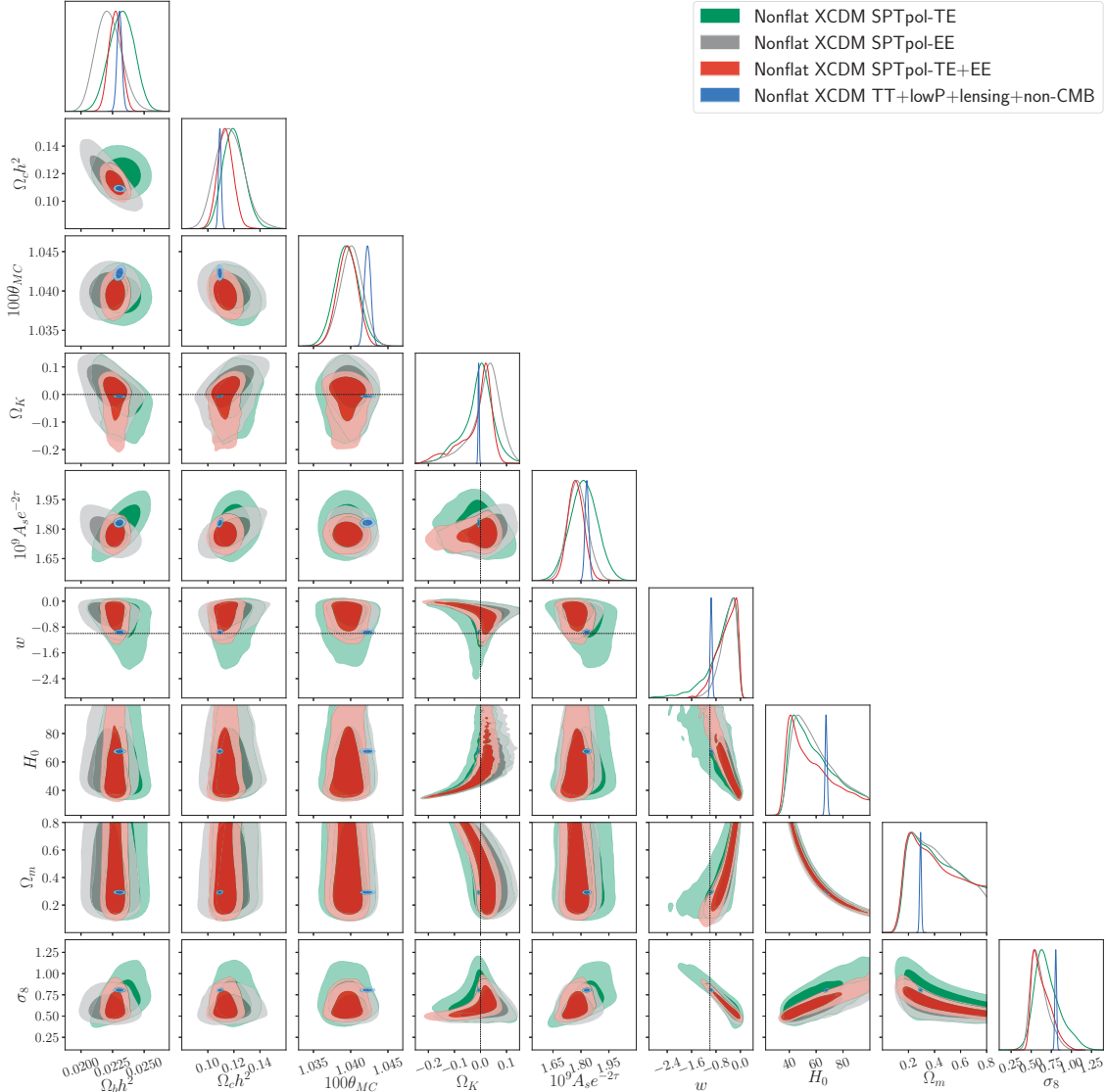


FIG. 8: Likelihood distributions of the untilted non-flat XCDM model parameters constrained by using the SPTpol TE+EE, TE, and EE data alone. For comparison, results from the Planck 2015 data (TT+lowP+lensing) together with non-CMB data sets (BAO, SN, $H(z)$, $f\sigma_8$) are also shown. Dotted straight lines indicate $w = -1$ or $\Omega_k = 0$.

and 2.7σ lower than what Planck does. This has been noted for the tilted flat Λ CDM model in Ref. [25]. By comparing the blue and red contours in the $\sigma_8-\Omega_m$ panels of Figs. 4–6 and Figs. 10–12 (even in Fig. 10 for the untilted non-flat Λ CDM model) we see that adding the SPTpol TE+EE data to the mix results in a slight shift of the contours in the direction that eases tension with weak lensing measurements. We emphasize however that this shift is not as significant as that caused by non-zero spatial curvature in the closed models, see Refs. [13–15, 17, 20, 21].

While the SPTpol data H_0 value is larger than the Planck 2015 CMB and non-CMB data H_0 value in the tilted flat Λ CDM model (first seen in Ref. [25]), this is not true in most of the other models. Additionally, adding

the SPTpol data to the Planck 2015 CMB and non-CMB data does not result in a significant change in the measured H_0 's, which are quite consistent with a number of recent H_0 estimates, [35].

While the PTEs in Tables IV and VII indicate no significant evidence for tension between models constrained using Planck 2015 CMB and non-CMB data and constrained using the SPTpol TE+EE data, the N_σ values are always larger than 2.2 and sometimes exceed 3. This means that CMB power spectra of the models that best fit the Planck 2018 data, the TT+lowP+lensing+non-CMB data, and the SPTpol TE+EE data do not provide good fits to the SPTpol TE+EE data. This is clearly illustrated in Figs. 13–14 that show the TT, TE, and EE power spectra that best fit the SPTpol TE+EE, TE, and

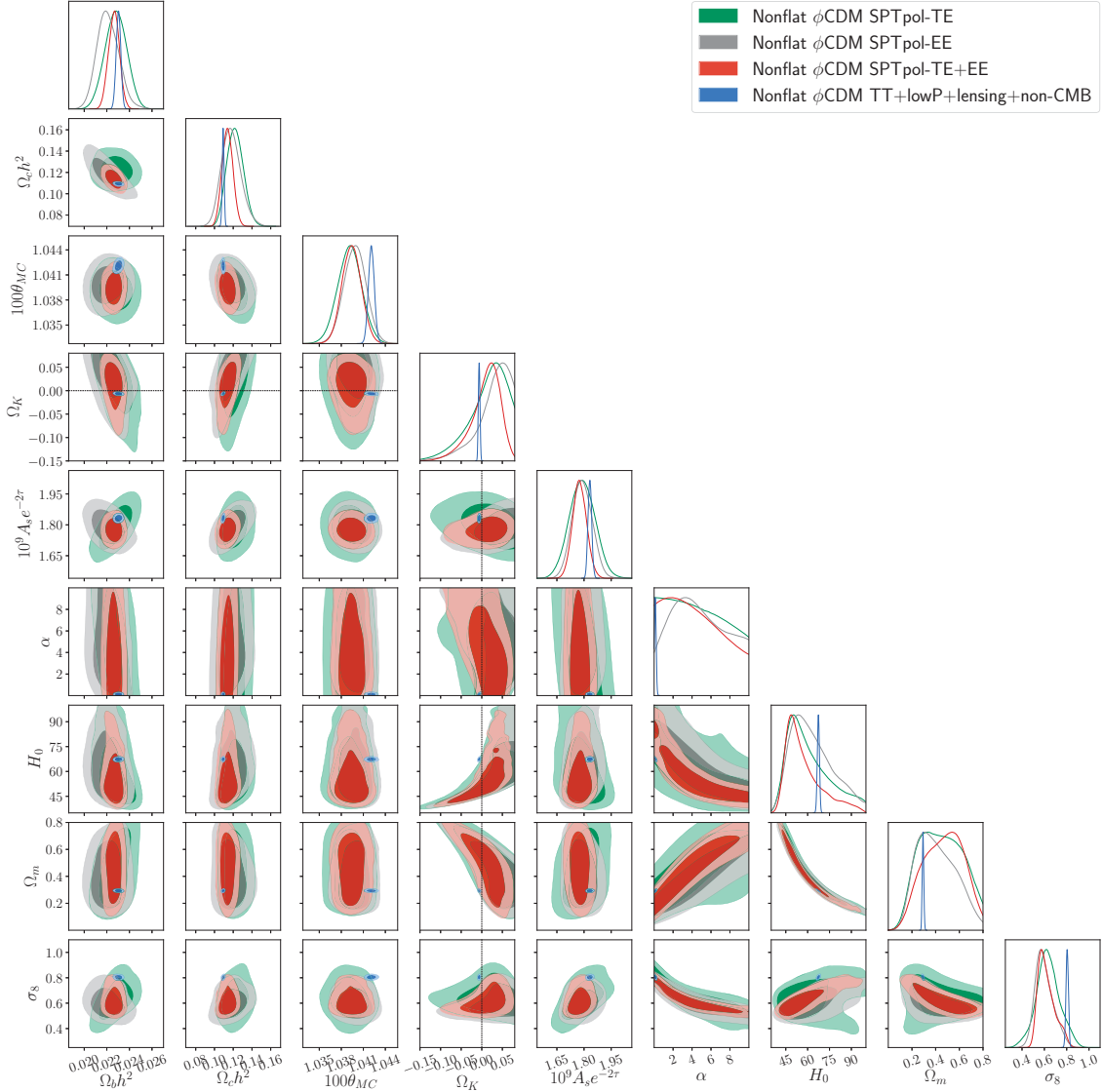


FIG. 9: Likelihood distributions of the untilted non-flat ϕ CDM model parameters constrained by using the SPTpol TE+EE, TE, and EE data alone. For comparison, results from the Planck 2015 data (TT+lowP+lensing) together with non-CMB data sets (BAO, SN, $H(z)$, $f\sigma_8$) are also shown. Dotted straight lines indicate $\Omega_k = 0$.

EE data sets in the various dark energy models, together with the difference and ratio of power spectrum with respect to the best-fit fiducial model constrained by using the Planck 2015 CMB and non-CMB data. From these figures we see that the best-fit models favored by the SPTpol data do not fit well the CMB temperature power spectrum in the low ℓ range ($\ell < 200$).

VI. SUMMARY

We have constrained tilted flat and untilted non-flat dark energy inflation models by using SPTpol CMB, Planck 2015 CMB, and non-CMB data. In each case we have considered three different dark energy models, a

time-independent cosmological constant as well as ideal X -fluid and scalar field dynamical dark energy density models.

In summary, our main findings are:

- All the Planck CMB and non-CMB data best-fit model CMB anisotropy power spectra we consider do not provide great fits to the SPTpol TE+EE data. Models that best-fit the Planck CMB and non-CMB data give larger minimum χ^2 when they try to fit the SPTpol data.
- In all models we consider, there is, however, no significant evidence of tension between a model constrained using Planck 2015 CMB and non-CMB data and the same model constrained using SPTpol

TABLE VI: Untilted non-flat Λ CDM, XCDM, ϕ CDM model parameters constrained by using Planck 2015, SPTpol TE+EE, and non-CMB data (mean and 68.3% confidence limits).

Untilted non-flat Λ CDM			
Parameter	TT+lowP+lensing+SPTpol	TT+lowP+lensing+non-CMB	TT+lowP+lensing+non-CMB+SPTpol
$\Omega_b h^2$	0.02303 ± 0.00018	0.02305 ± 0.00019	0.02303 ± 0.00018
$\Omega_c h^2$	0.1091 ± 0.0011	0.1093 ± 0.0010	0.1093 ± 0.0010
$100\theta_{\text{MC}}$	1.04206 ± 0.00039	1.04227 ± 0.00041	1.04201 ± 0.00039
τ	0.100 ± 0.021	0.112 ± 0.012	0.108 ± 0.011
Ω_k	-0.0139 ± 0.0086	-0.0083 ± 0.0016	-0.0080 ± 0.0016
$\ln(10^{10} A_s)$	3.107 ± 0.042	3.132 ± 0.022	3.123 ± 0.021
$10^9 A_s e^{-2\tau}$	1.829 ± 0.010	1.831 ± 0.010	1.8292 ± 0.0100
$H_0 [\text{km s}^{-1} \text{ Mpc}^{-1}]$	65.8 ± 3.4	68.01 ± 0.62	68.04 ± 0.61
Ω_m	0.309 ± 0.032	0.2875 ± 0.0055	0.2872 ± 0.0052
σ_8	0.799 ± 0.021	0.8121 ± 0.0095	0.8081 ± 0.0093
Untilted non-flat XCDM			
Parameter	TT+lowP+lensing+SPTpol	TT+lowP+lensing+non-CMB	TT+lowP+lensing+non-CMB+SPTpol
$\Omega_b h^2$	0.02304 ± 0.00018	0.02305 ± 0.00020	0.02304 ± 0.00018
$\Omega_c h^2$	0.1091 ± 0.0011	0.1092 ± 0.0010	0.1092 ± 0.0010
$100\theta_{\text{MC}}$	1.04208 ± 0.00039	1.04227 ± 0.00042	1.04199 ± 0.00039
τ	0.099 ± 0.021	0.119 ± 0.012	0.115 ± 0.012
Ω_k	-0.018 ± 0.018	-0.0069 ± 0.0020	-0.0066 ± 0.0019
w	-1.08 ± 0.40	-0.960 ± 0.032	-0.958 ± 0.032
$\ln(10^{10} A_s)$	3.104 ± 0.042	3.146 ± 0.024	3.137 ± 0.024
$10^9 A_s e^{-2\tau}$	1.829 ± 0.010	1.832 ± 0.010	1.830 ± 0.010
$H_0 [\text{km s}^{-1} \text{ Mpc}^{-1}]$	69 ± 15	67.45 ± 0.75	67.46 ± 0.76
Ω_m	0.32 ± 0.14	0.2923 ± 0.0066	0.2921 ± 0.0067
σ_8	0.82 ± 0.11	0.805 ± 0.011	0.801 ± 0.011
Untilted non-flat ϕ CDM			
Parameter	TT+lowP+lensing+SPTpol	TT+lowP+lensing+non-CMB	TT+lowP+lensing+non-CMB+SPTpol
$\Omega_b h^2$	0.02302 ± 0.00018	0.02304 ± 0.00020	0.02304 ± 0.00018
$\Omega_c h^2$	0.1091 ± 0.0010	0.1093 ± 0.0010	0.1092 ± 0.0010
$H_0 [\text{km s}^{-1} \text{ Mpc}^{-1}]$	54.7 ± 6.9	67.36 ± 0.72	67.36 ± 0.72
τ	0.102 ± 0.020	0.122 ± 0.012	0.117 ± 0.012
Ω_k	-0.034 ± 0.021	-0.0063 ± 0.0020	-0.0061 ± 0.0020
α [95.4% C.L.]	< 4.6	< 0.31	< 0.32
$10^9 A_s e^{-2\tau}$	1.828 ± 0.010	1.832 ± 0.010	1.830 ± 0.010
$100\theta_{\text{MC}}$	1.04186 ± 0.00039	1.04210 ± 0.00041	1.04183 ± 0.00039
Ω_m	0.47 ± 0.12	0.2931 ± 0.0064	0.2930 ± 0.0064
σ_8	0.707 ± 0.056	0.805 ± 0.011	0.800 ± 0.010

Note: Parameter constraints for Planck 2015 TT+lowP+lensing and non-CMB (SN, BAO, $H(z)$, $f\sigma_8$) data sets are from Refs. [13] for the Λ CDM and XCDM models and from Ref. [17] for the ϕ CDM model.

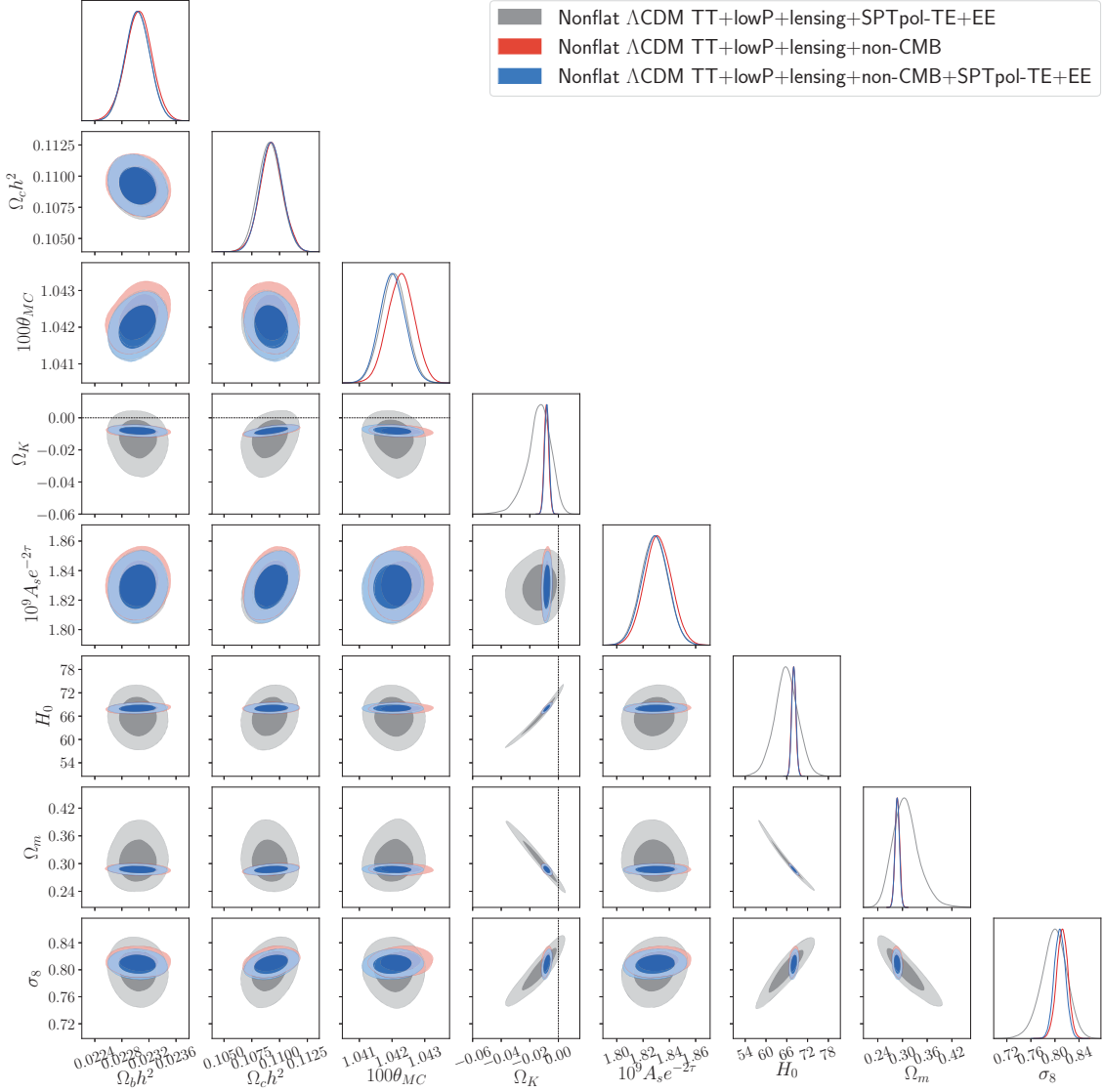


FIG. 10: Likelihood distributions of the untilted non-flat Λ CDM model parameters constrained by using Planck 2015 TT+lowP+lensing data, non-CMB data, and SPTpol TE+EE data. Dotted straight lines indicate $\Omega_k = 0$.

TE+EE data (i.e., given the uncertainties, in each model the cosmological parameter constraints from both sets of data are largely consistent with each other) and so it is appropriate to use these data together to jointly constrain model parameters. (We note that Ref. [25] found some tension between the tilted flat Λ CDM model constrained using just the Planck 2015 data and that constrained using the SPTpol TE+EE data.)

- Depending on cosmological model, the SPTpol TE+EE data can favor a larger or smaller H_0 than is favored by the Planck 2015 data.
- In most models the SPTpol TE+EE data favor a lower σ_8 than is favored by the Planck 2015 data and moves the $\sigma_8-\Omega_m$ Planck 2015 CMB and non-

CMB data contours in the direction of reducing tension with weak lensing measurements, but the overall effect is very small.

- When the smaller angular scale SPTpol TE+EE data is used to jointly analyze untilted non-flat models with the TT+lowP+lensing data or with the TT+lowP+lensing+non-CMB data, closed untilted models with non-zero Ω_k are still favored over the corresponding $\Omega_k = 0$ untilted cases.

Combined with the Planck CMB data, the non-CMB data, especially the BAO data, constrain the cosmological model parameters significantly better than do the SPTpol TE+EE data. While near-future ground-based CMB anisotropy experiments will produce data with better constraining power, perhaps data from a future space-

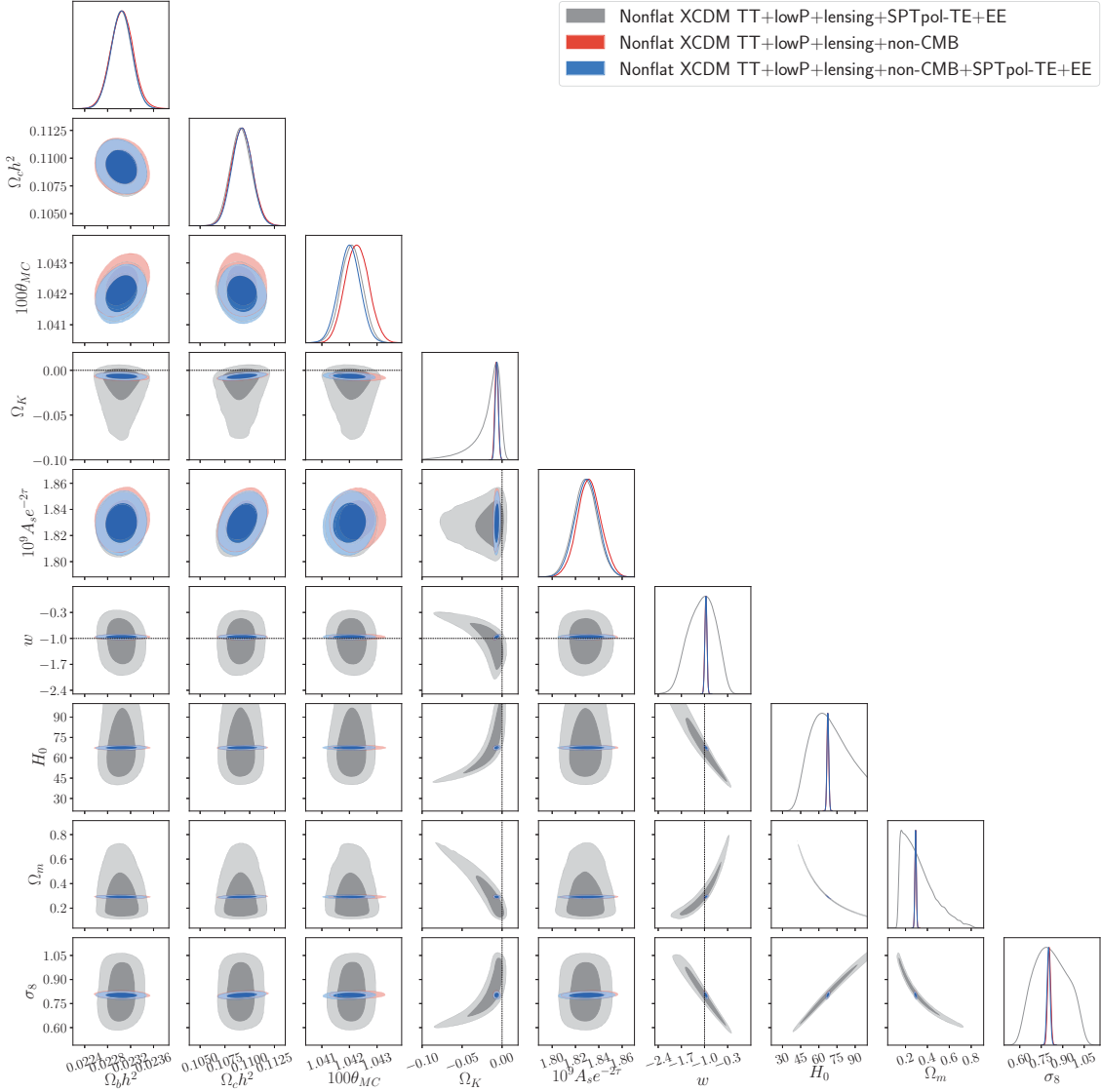


FIG. 11: Likelihood distributions of the untilted non-flat XCDM model parameters constrained by using Planck 2015 TT+lowP+lensing data, non-CMB data, and SPTpol TE+EE data. Dotted straight lines indicate $w = -1$ or $\Omega_k = 0$.

based experiment might be more helpful for this purpose.

Recently, there was a report that the Planck 2018 CMB spectra prefer a positive curvature at more than 99% confidence level [38]. According to the tilted nonflat Λ CDM model constraints of Ref. [38], a quite low value of Hubble constant is favored and Ω_m and σ_8 parameters constrained by the Planck CMB data have discordance with the cosmic shear measurements. On the other hand, our untilted nonflat dark energy models have a Hubble constant that is very similar to that of the flat Λ CDM model and give Ω_m and σ_8 values that are consistent with those from the weak lensing observations (see Refs. [13, 15, 17]).

It has been known that there are systematic difference between model parameters obtained with high ℓ and low ℓ Planck 2015 data [39, 40]. In addition, the South Pole Telescope team reported that there might be inconsis-

tencies between the SPT CMB temperature anisotropy and the Planck 2015 high ℓ data in the tilted flat Λ CDM model [41]. Such tension between parameter constraints for the Planck and SPTpol data sets is reduced when the gravitational lensing scaling parameter A_L is introduced as a free parameter [25]. Whether these tensions persist in other dark energy models will be investigated in a subsequent study.

Acknowledgments

C.-G.P. was supported by the Basic Science Research Program through the National Research Foundation of Korea (NRF) funded by the Ministry of Education (No. 2017R1D1A1B03028384). B.R. was supported in part by

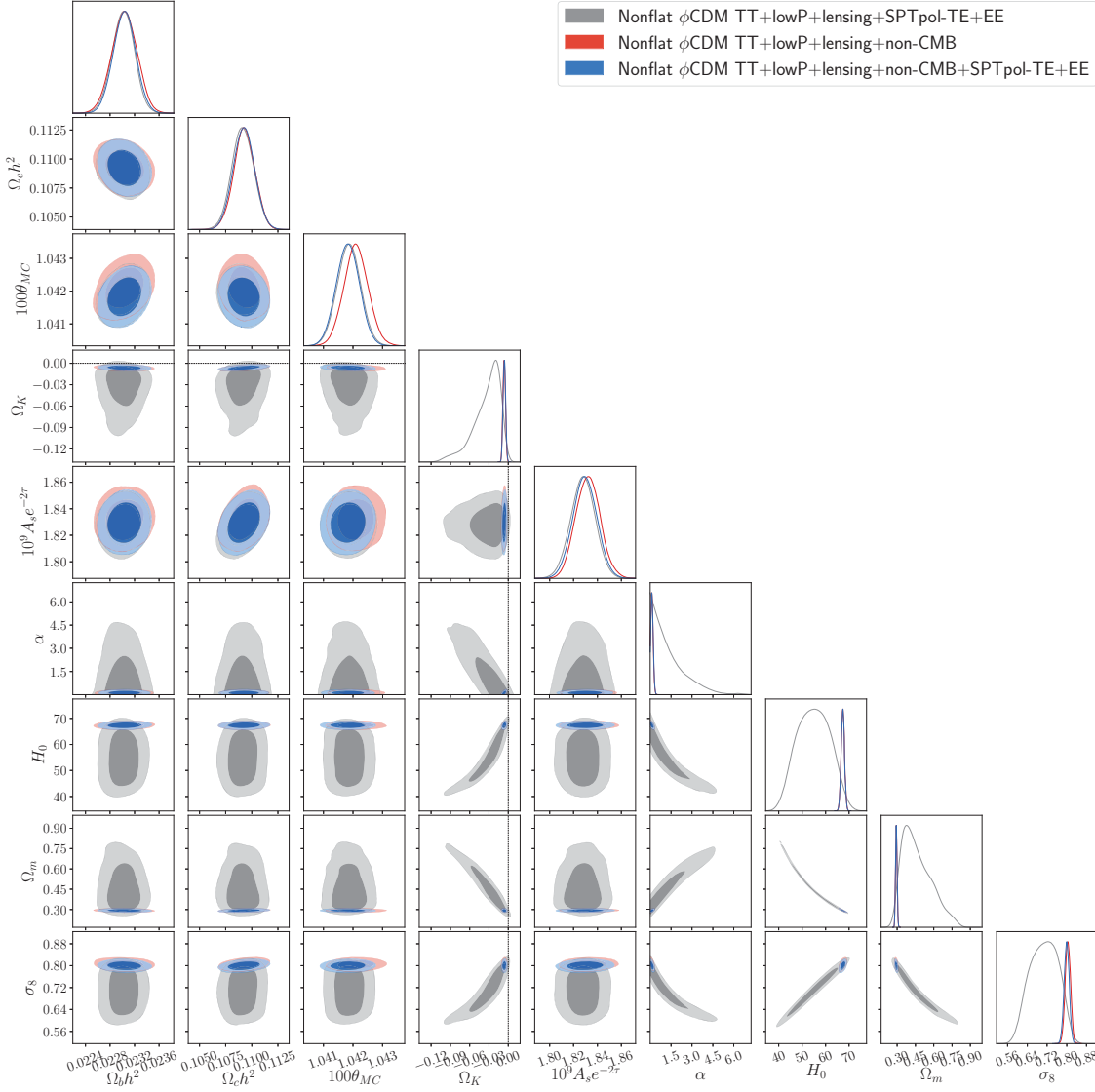


FIG. 12: Likelihood distributions of the untilted non-flat ϕ CDM model parameters constrained by using Planck TT+lowP+lensing data, non-CMB data, and SPTpol TE+EE data. Dotted straight lines indicate $\Omega_K = 0$.

DOE grant de-sc0019038.

- [1] P. J. E. Peebles, *Astrophys. J.* **284**, 439 (1984).
- [2] P. A. R. Ade et al., *Astron. Astrophys.* **594**, A13 (2016) [arXiv:1502.01589].
- [3] N. Aghanim et al., arXiv:1807.06209.
- [4] D. M. Scolnic et al., *Astrophys. J.* **859**, 101 (2018) [arXiv:1710.00845].
- [5] S. Alam et al., *Mon. Not. R. Astro. Soc.* **470**, 2617 (2017) [arXiv:1607.03155].
- [6] F. Beutler, C. Blake, M. Colless et al., *Mon. Not. R. Astron. Soc.* **416**, 3017 (2011) [arXiv:1106.3366].
- [7] A. J. Ross, L. Samushia, C. Howlett et al., *Mon. Not. R. Astron. Soc.* **449**, 835 (2015) [arXiv:1409.3242].
- [8] M. Ata, F. Baumgarten, J. Bautista et al., *Mon. Not. R. Astron. Soc.* **473**, 4773 (2018) [arXiv:1705.06373].
- [9] J. E. Bautista, N. G. Busca, J. Guy et al., *Astron. Astrophys.* **603**, A12 (2017) [arXiv:1702.00176].
- [10] A. Font-Ribera, D. Kirkby, N. Busca et al. *J. Cosmol. Astropart. Phys.* **1405**, 027 (2014) [arXiv:1311.1767].
- [11] M. Moresco et al., *JCAP*, **1605**, 014 (2016) [arXiv:1601.01701].
- [12] O. Farooq, F. R. Madiyar, S. Crandall, and B. Ratra, *Astrophys. J.* **835**, 26 (2017) [arXiv:1607.03537].
- [13] C.-G. Park and B. Ratra, *Astrophys. Space Sci.* **364**, 82 (2019) [arXiv:1803.05522].
- [14] J. Ooba, B. Ratra, and N. Sugiyama, *Astrophys. J.* **864**, 80 (2018) [arXiv:1707.03452].

TABLE VII: Minimum χ^2 values for the SPTpol TE+EE, TE, EE spectra in the best-fit untilted non-flat Λ CDM, XCDM, and ϕ CDM models constrained by using Planck 2015 TT+lowP+SN+BAO+ $H(z)$ + $f\sigma_8$ data [13, 17].

		Best-fit untilted non-flat Λ CDM		SPT (Λ CDM τ [13])			
SPTpol spectrum	N_b	χ^2_{\min}	N_σ	χ^2_{\min}	N_σ	χ_p^2	PTE
TE + EE	112	146.96	2.98	136.18	2.23	10.31	0.067
TE	56	73.88	2.64	68.72	2.11	4.09	0.536
EE	56	68.46	2.09	59.05	1.13	6.73	0.242
		Best-fit untilted non-flat XCDM		SPT (XCDM τ [13])			
SPTpol spectrum	N_b	χ^2_{\min}	N_σ	χ^2_{\min}	N_σ	χ_p^2	PTE
TE + EE	112	147.46	3.10	136.45	2.33	8.24	0.221
TE	56	74.14	2.80	68.81	2.25	4.34	0.630
EE	56	68.78	2.25	58.85	1.22	9.01	0.173
		Best-fit untilted non-flat ϕ CDM		SPT (ϕ CDM τ [17])			
SPTpol spectrum	N_b	χ^2_{\min}	N_σ	χ^2_{\min}	N_σ	χ_p^2	PTE (H_0)
TE + EE	112	146.81	3.05	137.34	2.39	6.45	0.375
TE	56	73.80	2.76	69.32	2.30	5.30	0.506
EE	56	68.43	2.21	60.22	1.36	7.58	0.270
SPTpol spectrum	N_b	χ^2_{\min}	N_σ	χ^2_{\min}	N_σ	χ_p^2	PTE (θ_{MC})
TE + EE	112	146.81	3.05	137.34	2.39	10.19	0.117
TE	56	73.80	2.76	69.32	2.30	6.93	0.328
EE	56	68.43	2.21	60.22	1.36	8.88	0.181

Note: We assume a different Gaussian prior of τ for each cosmological model. For our best-fit untilted non-flat Λ CDM, XCDM, and ϕ CDM models, we apply $\tau = 0.112 \pm 0.012$, 0.119 ± 0.012 , and 0.122 ± 0.012 [13, 17], respectively.

- [15] C.-G. Park and B. Ratra, *Astrophys. J.* **882**, 158 (2019) [arXiv:1801.00213 [astro-ph.CO]].
- [16] J. Ooba, B. Ratra, and N. Sugiyama, *Astrophys. Space Sci.* **364**, 176 (2019) [arXiv:1802.05571].
- [17] C.-G. Park and B. Ratra, *Astrophys. J.* **868**, 83 (2018) [arXiv:1807.07421].
- [18] Earlier discussions of observational constraints on dark energy dynamics may be traced through G. Chen and B. Ratra, *Astrophys. J.* **612**, L1 (2004) [arXiv:astro-ph/045636]; L. Samushia, G. Chen, and B. Ratra, arXiv:0706.1963; M. Yashar, B. Bozek, A. Abrahamse, A. Albrecht, and N. Barnard, *Phys. Rev. D* **79**, 103004 (2009) [arXiv:0811.2253]; L. Samushia and B. Ratra, *Astrophys. J.* **714**, 1347 (2010) [arXiv:0905.3836]; Y. Chen and B. Ratra, *Phys. Lett. B* **703**, 406 (2011) [arXiv:1106.4294]; L. Campanelli, G.-L. Fogli, T. Kahnishvili, A. Marrone, and B. Ratra, *Eur. Phys. J.* **C72**, 2218 (2012) [arXiv:1110.2310]; O. Farooq and B. Ratra, *Astrophys. J.* **766**, L7 (2013) [arXiv:1301.5243]; O. Farooq, S. Crandall, and B. Ratra, *Phys. Lett. B* **726**, 72 (2013) [arXiv:1305.1957]; O. Avsajanishvili, L. Samushia, N. A. Arkhipova, and T. Kahnishvili, arXiv:1511.09317; J. Solà, A. Gómez-Valent, and J. de Cruz Pérez, *Mod. Phys. Lett. A* **32**, 1750054 (2017) [arXiv:1610.08965]; J. Solà, J. de Cruz Pérez, and A. Gómez-Valent, *Mon. Not. R. Astro. Soc.* **478**, 4357 (2018) [arXiv:1703.08218]; Z. Zhai, M. Blanton, A. Slosar, and J. Tinker, *Astrophys. J.* **850**, 183 (2017) [arXiv:1705.10031]; A. Sangwan, A. Tripathi, and H. K. Jassal, arXiv:1804.09350; J. Ryan, S. Doshi, and B. Ratra, *Mon. Not. R. Astro. Soc.* **480**, 759 (2018) [arXiv:1805.06408]; J. Solà Peracaula, A. Gómez-Valent, and J. de Cruz Pérez, *Phys. Dark Univ.* **25**, 100311 (2019) [arXiv:1811.03505]; A. Singh, A. Sangwan, and H. K. Jassal, *JCAP* **1904**, 047 (2019) [arXiv:1811.07513]; S. Mitra, C.-G. Park, T. R. Choudhury, and B. Ratra, *Mon. Not. R. Astro. Soc.* **487**, 5118 (2019) [arXiv:1901.09927], and references therein.
- [19] P. J. E. Peebles and B. Ratra, *Astrophys. J.* **325**, L17 (1988); B. Ratra and P. J. E. Peebles, *Phys. Rev. D* **37**, 3406 (1988); A. Pavlov, S. Westmoreland, K. Saaidi, and B. Ratra, *Phys. Rev. D* **88**, 123513 (2013) [arXiv:1307.7399].
- [20] J. Ooba, B. Ratra, and N. Sugiyama, *Astrophys. J.* **869**, 34 (2018) [arXiv:1710.03271].

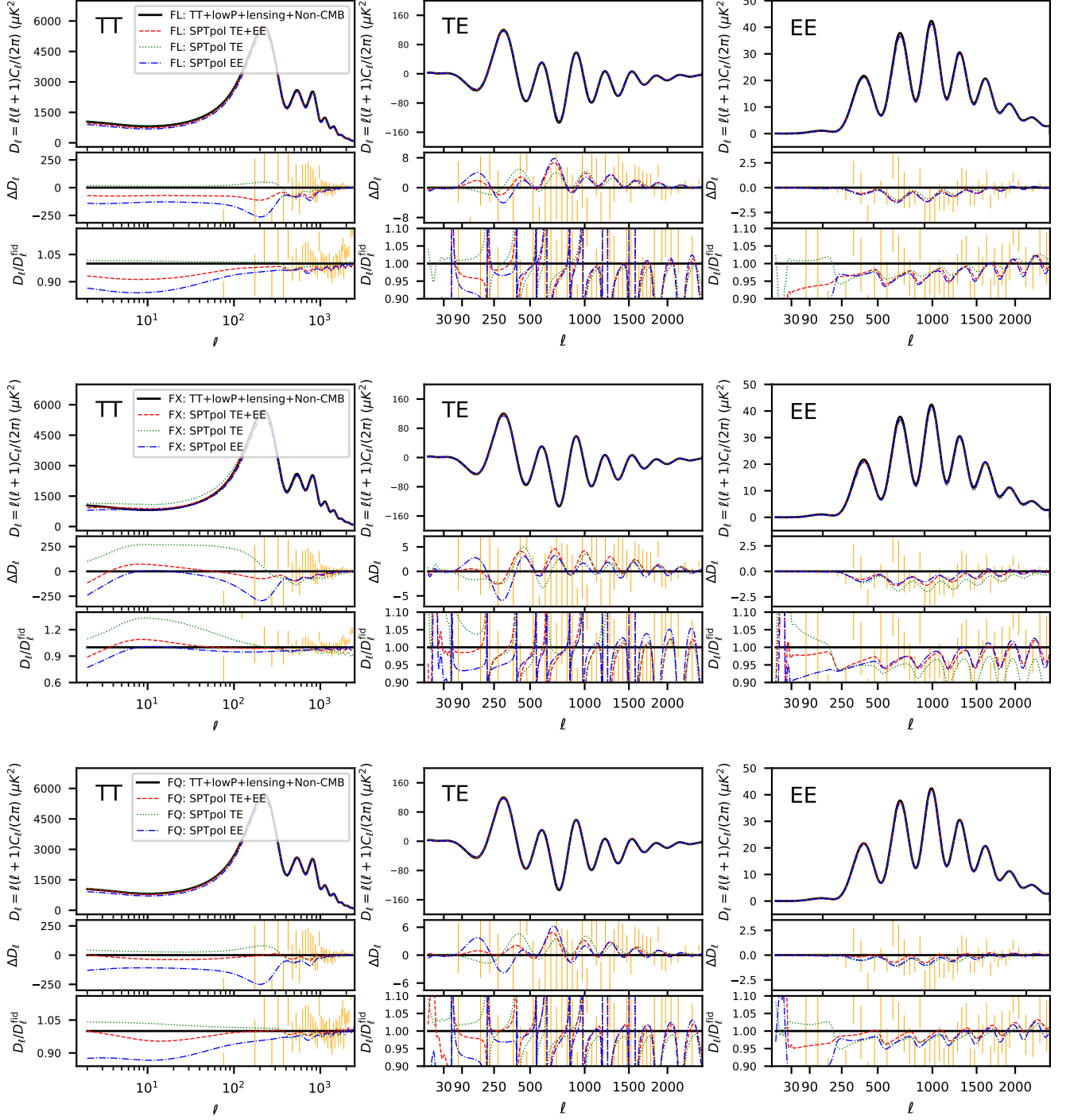


FIG. 13: CMB power spectra of best-fit tilted flat Λ C CDM (FL, upper row), XCDM (FX, middle row), and ϕ C CDM (FQ, lower row) models constrained by using TT+lowP+lensing+non-CMB data, and SPTpol TE+EE, TE, and EE data sets. Difference (ΔD_ℓ) and ratio ($D_\ell/D_\ell^{\text{fid}}$) panels show quantities with respect to the fiducial model constrained using TT+lowP+lensing+non-CMB data. Vertical error bars indicate the confidence limits of the SPTpol power spectrum data including TT band powers.

- [21] J. Ooba, B. Ratra, and N. Sugiyama, *Astrophys. J.* **866**, 68 (2018) [arXiv:1712.08617].
- [22] Earlier discussions of observational constraints on spatial curvature may be traced through O. Farooq, D. Mania, and B. Ratra, *Astrophys. Space Sci.* **357**, 11

- (2015) [arXiv:1308.0834]; Y. Chen, B. Ratra, M. Biesiada, S. Li, and Z.-H. Zhu, *Astrophys. J.* **829**, 61 (2016) [arXiv:1603.07115]; H. Yu and F. Y. Wang, *Astrophys. J.* **828**, 85 (2016) [arXiv:1605.02483]; J.-J. Wei and X.-F. Wu, *Astrophys. J.* **838**, 160 (2017) [arXiv:1611.07196];

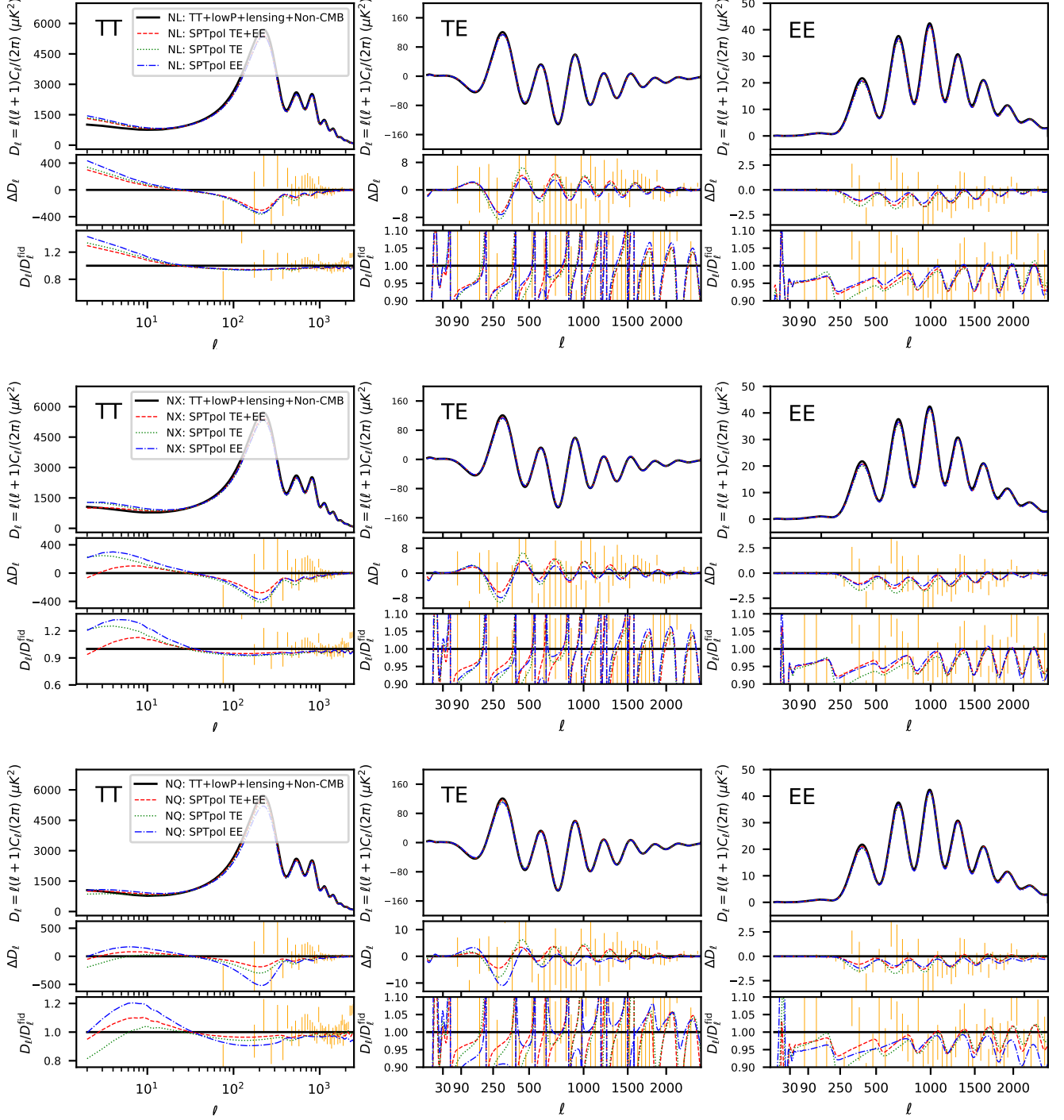


FIG. 14: CMB power spectra of best-fit untilted Λ CDM (NL, upper row), XCDM (NX, middle row), and ϕ CDM (NQ, lower row) models constrained by using TT+lowP+lensing+non-CMB data, and SPTpol TE+EE, TE, and EE data sets. Difference (ΔD_ℓ) and ratio ($D_\ell/D_\ell^{\text{fid}}$) panels show quantities with respect to the fiducial model constrained using TT+lowP+lensing+non-CMB data. Vertical error bars indicate the confidence limits of the SPTpol power spectrum data including TT band powers.

- A. Rana, D. Jain, S. Mahajan, and A. Mukherjee, JCAP, **1703**, 028 (2017) [arXiv:1611.07196]; A. Witzemann et al., Mon. Not. R. Astro. Soc. **477**, L122 (2018) [arXiv:1711.02179]; H. Yu, B. Ratra, and F.-Y. Wang, Astrophys. J. **856**, 3 (2018) [arXiv:1711.03437]; S. Mitra, T. R. Choudhury, and B. Ratra, Mon. Not. R. Astro. Soc. **479**, 4566 (2018) [arXiv:1712.00018], and references therein. More recent developments may be found in J. Penton, J. Peyton, A. Zahoor, and B. Ratra, Publ. Astron. Soc. Pac. **130**, 114001 (2018) [arXiv:1808.01490]; C.-G. Park and B. Ratra, Astrophys. Space Sci. **364**, 134 (2019) [arXiv:1809.03598]; S. Akama and T. Kobayashi, Phys. Rev. D **99**, 043522 (2019) [arXiv:1810.01863]; T. M. C. Abbott et al., Phys. Rev. D **99**, 123505 (2019) [arXiv:1810.02699]; H. Xu, Z. Huang, Z. Liu, and H. Miao, Astrophys. J. **877**, 107 (2019) [arXiv:1812.09100]; J. Zheng, F. Melia, and T.-J. Zhang, arXiv:1901.05705; C.-Z. Ruan, F. Melia, Y. Chen, and T.-J. Zhang, Astrophys. J. **881**, 132 (2019) [arXiv:1901.06626]; S. D. Odintsov and V. K. Oikonomou, Class. Quant. Grav. **36**, 065008 (2019) [arXiv:1902.01422]; J. Ryan, Y. Chen, and B. Ratra, Mon. Not. R. Astro. Soc. **488**, 3844 (2019) [arXiv:1902.03196]; E.-K. Li, M. Du, and L. Xu, Mon. Not. R. Astro. Soc. **491**, 4960 (2019) [arXiv:1903.11433]; R. Giambò, J. Mirizzi, and A. Pezzola, arXiv:1905.01742; A. A. Coley, arXiv:1905.04588; M. Eingorn, A. E. Yukselci, and A. Zhuk, Eur. Phys. J. C **79**, 655 (2019) [arXiv: 1905.09502]; J. F. Jesus, R. Valentim, P. H. R. S. Moraes, and M. Malheiro, arXiv:1907.01033; C. R. Farrugia and J. Sultana, Int. J. Mod. Phys. D **26**, 1750115 (2017) [arXiv:1907.07651]; W. Handley, Phys. Rev. D **100**, 123517 (2019) [arXiv:1907.08524]; N. Khadka and B. Ratra, Mon. Not. R. Astro. Soc. **492**, 4456 (2019) [arXiv:1909.01400], and references therein.
- [23] S. Das et al., JCAP **1404**, 014 (2014) [arXiv:1301.1037].
- [24] K. T. Story et al., Astrophys. J. **779**, 86 (2013) [arXiv:1210.7231]; E. M. George et al., Astrophys. J. **799**, 177 (2015) [arXiv:1408.3161].
- [25] J. W. Henning et al., Astrophys. J. **852**, 97 (2018) [arXiv:1707.09353].
- [26] B. Ratra et al., Astrophys. J. **517**, 549 (1999) [arXiv:astro-ph/9901014].
- [27] A. Challinor and A. Lasenby, Astrophys. J. **513**, 1 (1999) [arXiv:astro-ph/9804301]; A. Lewis, A. Challinor, and A. Lasenby, Astrophys. J. **538**, 473 (2000) [arXiv:astro-ph/9911177]; A. Lewis and S. Bridle, Phys. Rev. D **66**, 103511 (2002) [arXiv:astro-ph/0205436].
- [28] F. Lucchin and S. Matarrese, Phys. Rev. D **32**, 1316 (1985); B. Ratra, Phys. Rev. D **45**, 1913 (1992); Phys. Rev. D **40**, 3939 (1989).
- [29] J. R. Gott, Nature **295**, 304 (1982).
- [30] S. W. Hawking, Nucl. Phys. B **239**, 257 (1984); B. Ratra, Phys. Rev. D **31**, 1931 (1985).
- [31] B. Ratra and P. J. E. Peebles, Phys. Rev. D **52**, 1837 (1995).
- [32] B. Ratra, Phys. Rev. D **96**, 103534 (2017) [arXiv:1707.03439].
- [33] C. G. Park and B. Ratra, Astrophys. Space Sci. **364**, 134 (2019) [arXiv:1809.03598].
- [34] In the last panel of Table IV (VII), for the tilted flat (untilted non-flat) ϕ CDM model, the numerical values in the upper half of this panel assume θ_{MC} as a dependent parameter and H_0 as a free parameter (see discussion in Ref. [17]) while the numerical values in the lower half of this panel assume H_0 as a dependent parameter and θ_{MC} as a free parameter, as is assumed in the Λ CDM and XCDM cases that are also shown in the table.
- [35] See J. R. Gott, M. S. Vogeley, S. Podariu, and B. Ratra, Astrophys. J. **549**, 1 (2001) [arXiv:astro-ph/0006103]; G. Chen, J. R. Gott, and B. Ratra, Publ. Astron. Soc. Pac. **115**, 1269 (2003) [arXiv:astro-ph/0308099]; G. Chen and B. Ratra, Publ. Astron. Soc. Pac. **123**, 1127 (2011) [arXiv:1105.5206] for early indications from median statistics analyses of Huchra's large compilations of H_0 measurements. For recent measurements of H_0 see B. L'Huillier and A. Shafieloo, JCAP **1701**, 015 (2017) [arXiv:1606.06832]; Y. Chen, S. Kumar, and B. Ratra, Astrophys. J. **835**, 86 (2017) [arXiv:1606.07316]; B. R. Zhang et al., Mon. Not. R. Astro. Soc. **471**, 2254 (2017) [arXiv:1706.07573]; Y. Wang, L. Xu, and G.-B. Zhao, Astrophys. J. **849**, 84 (2017) [arXiv:1706.09149]; S. Dhawan, S. W. Jha, and B. Leibundgut, Astron. Astrophys. **609**, A72 (2017) [arXiv:1707.00715]; W. Lin and M. Ishak, Phys. Rev. D **96**, 083532 (2017) [arXiv:1708.09813]; D. Fernández Arenas et al., Mon. Not. R. Astro. Soc. **474**, 1250 (2018) [arXiv:1710.05951]; T. M. C. Abbott et al., Mon. Not. R. Astro. Soc. **480**, 3879 (2018) [arXiv:1711.00403]; A. Gómez-Valent and L. Amendola, JCAP **1804**, 051 (2018) [arXiv:1802.01505]; B. S. Haridasu, V. V. Luković, M. Moresco, and N. Vittorio, JCAP **1810**, 015 (2018) [arXiv:1805.03595]; J. Zhang, Publ. Astron. Soc. Pac. **130**, 084502 (2018); X. Zhang and Q. G. Huang, Commun. Theor. Phys. **71**, 826 (2019) [arXiv:1812.01877]; A. Domínguez et al., Astrophys. J. **885**, 137 (2019) [arXiv:1903.12097], and references therein. We emphasize however that some local expansion rate measurements give a higher H_0 value, see A. G. Riess et al., Astrophys. J. **876**, 85 (2019) [arXiv:1903.07603], and references therein.
- [36] Planck Collaboration 2015, *Planck 2015 Results: Cosmological Parameter Tables* at wiki.cosmos.esa.int/planckpla2015/images/f/f7/Baseline_params_table_2015_limit68.pdf
- [37] For a more quantitative analysis, we can compute the deviance information criterion (DIC) [see D. J. Spiegelhalter, N. G. Best, B. P. Carlin and A. van der Linde, J. Roy. Statist. Soc. B **64**, 583 (2002)] to compare the tilted flat and untilted non-flat dark energy models constrained by using the SPTpol data. Given the likelihood function $P(d|\theta)$ with d data and θ model parameters, the DIC is defined as $DIC = D(\bar{\theta}) + 2p_D$, where $D(\theta) = -2 \ln(P(d|\theta)) + C$ (C is a constant), $p_D = \overline{D(\theta)} - D(\bar{\theta})$, and $\bar{\theta}$ indicates the expectation of θ . The model with a smaller DIC value is preferred over the model with a larger DIC value. For the tilted flat Λ CDM, XCDM, and ϕ CDM models constrained with SPTpol TE+EE data, we obtain $DIC = 171.76$ ($p_D = 17.42$), 171.87 ($p_D = 18.28$), and 166.44 ($p_D = 13.58$), respectively. For the untilted non-flat Λ CDM, XCDM, and ϕ CDM models constrained with the same data, $DIC = 170.30$ ($p_D = 17.06$), 170.84 ($p_d = 17.20$), and 169.52 ($p_d = 16.09$), respectively.
- [38] E. Di Valentino, A. Melchiorri and J. Silk, Nat. Astron. (2019) [arXiv:1911.02087].
- [39] G. E. Addison et al., Astrophys. J. **818**, 132 (2016) [arXiv:1511.00055].

- [40] N. Aghanim et al., *Astron. Astrophys.* **607**, A95 (2017) [arXiv:1608.02487].
- [41] K. Aylor et al., *Astrophys. J.* **850**, 101 (2017)